Geophys. J. Int. (2007) **170,** 417–435 doi: 10.1111/j.1365-246X.2007.03337.x

A three-dimensional geophysical model of the crust in the Barents Sea region: model construction and basement characterization

Oliver Ritzmann,[1] Nils Maercklin,[2] Jan Inge Faleide,[1,2] Hilmar Bungum,[2] Walter D. Mooney[3] and Shane T. Detweiler[3]

[1] *University of Oslo,* PO Box 1047 *Blindern,* 0316 *Oslo, Norway. E-mail: oliver.ritzmann@geo.uio.no*
[2] *NORSAR,* PO Box 53, 2027 *Kjeller, Norway*
[3] *US Geological Survey,* 345 *Middlefield Rd.,* MS 977, *Menlo Park, CA, USA*

Accepted 2006 December 18. Received 2006 December 18; in original form 2006 February 28

SUMMARY

BARENTS50, a new 3-D geophysical model of the crust in the Barents Sea Region has been developed by the University of Oslo, NORSAR and the U.S. Geological Survey. The target region comprises northern Norway and Finland, parts of the Kola Peninsula and the East European lowlands. Novaya Zemlya, the Kara Sea and Franz-Josef Land terminate the region to the east, while the Norwegian-Greenland Sea marks the western boundary. In total, 680 1-D seismic velocity profiles were compiled, mostly by sampling 2-D seismic velocity transects, from seismic refraction profiles. Seismic reflection data in the western Barents Sea were further used for density modelling and subsequent density-to-velocity conversion. Velocities from these profiles were binned into two sedimentary and three crystalline crustal layers. The first step of the compilation comprised the layer-wise interpolation of the velocities and thicknesses. Within the different geological provinces of the study region, linear relationships between the thickness of the sedimentary rocks and the thickness of the remaining crystalline crust are observed. We therefore, used the separately compiled (area-wide) sediment thickness data to adjust the total crystalline crustal thickness according to the total sedimentary thickness where no constraints from 1-D velocity profiles existed. The BARENTS50 model is based on an equidistant hexagonal grid with a node spacing of 50 km. The *P*-wave velocity model was used for gravity modelling to obtain 3-D density structure. A better fit to the observed gravity was achieved using a grid search algorithm which focussed on the density contrast of the sediment-basement interface. An improvement compared to older geophysical models is the high resolution of 50 km. Velocity transects through the 3-D model illustrate geological features of the European Arctic. The possible petrology of the crystalline basement in western and eastern Barents Sea is discussed on the basis of the observed seismic velocity structure. The BARENTS50 model is available at http://www.norsar.no/seismology/barents3d/.

Key words: Barents Sea, crustal structure, density, Moho discontinuity, sedimentary basin, seismic velocities.

1 INTRODUCTION

1.1 Intention

3-D seismic models of the Earth's crust and mantle play important roles in the correct location of seismic events. Seismic waves that cross the Moho discontinuity from below experience traveltime delays, since the crust has relatively low seismic velocities compared to the upper mantle. The crustal structure often contains inhomogeneities such as sedimentary basins with very low seismic velocities; in marine environments fine-grained sediments at the sea bottom may have *P*-wave velocities close to the speed of sound in water. Accurate velocity models of the crust and upper mantle are, therefore, required tools for seismic event detection, location, discrimination, source inversion and for subsequent traveltime modelling. Once a 3-D model is extended by the addition of other physical rock properties, such as the *S*-wave velocity, the density structure or the Q structure, it will also provide general capabilities for lithological and geological interpretations.

Previously, velocity models were developed at a variety of scales, such as local, regional, plate or global scales. They were based on a variety of methods, such as body and surface wave tomography, receiver function analysis, thermodynamic modelling or, as carried out here, by compiling first-order velocity data from active-source

seismic refraction experiments. The data coverage eventually limits the model quality, particularly since crustal seismic experiments usually are unevenly distributed. The velocity compilation for the Barents Sea region, as documented in this paper, is based on a large amount of first-order data. The onshore regions of Fennoscandia and European Russia have been explored by various older surveys (e.g. FENNOLORA, Guggisberg *et al.* 1991; POLAR, Luosto *et al.* 1989) while the Barents Sea-Svalbard region has been targeted in more recent studies (e.g. Breivik *et al.* 2002; Sakoulina *et al.* 2003; Ritzmann *et al.* 2004). In addition to these investigations, considerable amounts of seismic reflection data with up to 19 s recording time were acquired in the western Barents Sea (Gudlaugsson *et al.* 1987). The extensive data set available in the Barents Sea region is the basis for our new velocity model with a higher resolution (i.e. 50 km) than provided by earlier studies. Our goal has been to provide the best model the data allows, precise enough both for further basic geological research and for the detection, location and characterization of smaller events in the greater Barents Sea region.

The compilation strategy for the BARENTS50 model has been as follows: We collected all available velocity data based on seismic refraction experiments in the target region. A number of profiles were obtained from density modelling along deep seismic reflection profiles and subsequent density-to-velocity conversion. Subsequently, the seismic velocities and layer thicknesses were interpolated layer-by-layer. We observed different linear relationships between the sediment thickness and the thickness of the crystalline crust in the different provinces of our target region. A compiled sediment thickness map was used to adjust the crystalline crustal thicknesses where no database constraints were given. The 3-D velocity structure was then converted into density and used for gravity modelling, to obtain the 3-D density structure. A programmed grid search algorithm helped to obtain a better fit to the observed gravity field. The 3-D model of Levshin *et al.* (2005) was used to extend our model into the upper mantle. The *S*-wave structure for the crustal section was estimated using crustal *P*/*S*-wave ratios from same model.

1.2 The target region

The target region for this study covers about 3 million km^2 in the northern European Arctic (Fig. 1). The maximum longitudinal and latitudinal extent is *ca*. 2000 and 1800 km, respectively. Most of the region is within the territories of Norway and Russia. The Barents Sea is surrounded by the landscapes of northern Norway, Finland and the Kola Peninsula, the East-European lowlands, Novaya Zemlya and the Kara Sea, Franz-Josef Land, Svalbard Archipelago and the Norwegian-Greenland Sea. About 20 per cent of the target region is onshore with elevations up to 900 m while the remaining offshore parts are mostly shallow with 50–400 m depth in the Barents and Kara Seas. Only about 10 per cent of the region lies oceanward of the continent–ocean transition, where water depths are up to 4000 m.

1.3 Geological history

The geological elements in the target region developed throughout a large time span from the Early Archean to the late Cenozoic and can be subdivided as follows.

(i) The oldest rocks in the greater Barents Sea region are of Archean/Proterozoic age and are found on the Kola Peninsula and surrounding provinces (Fig. 1). Autochthon complexes of various ages form the northeastern part of the Fennoscandian Shield. Archean gneisses on the Kola Peninsula are separated by lower-grade greenstone belts. Granulite belts terminate this province against the Caledonian nappes of northern Norway to the west. Southwards towards the Gulf of Bothnia, early Proterozoic granites and granodiorites of the (Sveco-) Karelian Orogen are observed. Terrane accretion took place in the late Archean or early Proterozoic (Dobrhzhinetskaya *et al.* 1995). Further ancient rock formations are the Proterozoic basement provinces of the northeastern and southern Svalbard Archipelago (locally also Archean; Harland 1997).

(ii) The Caledonian Orogen extends along western Norway. Here, four tectonic nappes were thrust over Precambrian rocks of the Fennoscandian/Baltic Shield (Roberts & Gee 1985). Obduction of the Finnmarkian Belt started in the Caledonides in Vendian to Middle Cambrian times. Later, the Ordovician-Silurian Scandian Belt was obducted (Ramsay *et al.* 1985). Caledonian main thrusts are also revealed in the western Barents Sea, shown in Transect A–A′ at km 1400 and km 1000 (Fig. 1). The latter thrust strikes subparallel to the main Caledonian deformation front and post-Caledonian rift structures in the western Barents Sea (Fig. 1) and may connect Fennoscandia to a further micro-continent between Svalbard and Franz-Josef Land. Franz-Josef Land was separated into numerous tectonic blocks during the Caledonian orogeny (Dibner 1998) and simultaneous deformation is also reported from Svalbard.

(iii) The Pechora Basin developed between the Vendian Timan Ridge, a collision structure between the Baikalia/Fennoscandia and the Uralian Foldbelt south of Novaya Zemlya (Fig. 1; Zonenshain *et al.* 1990). Results from subsidence modelling point to an earlier start of the rifting history here than in the South Barents Basin in the Early Ordovician period (O'Leary *et al.* 2004). Later Devonian and Permo-Triassic rifting is established in both basins. The latter subsidence phase was more pronounced in the South Barents Basin and towards the foreland basins west of the Ural Foldbelt. Thick Mesozoic sedimentary rocks were deposited throughout the entire eastern Barents Sea and the total thickness of the sedimentary succession in the South Barents Sea basin possibly exceeds 20 km. Several authors proposed windows of oceanic crust (e.g. Zonenshain *et al.* 1990) for the crystalline crust below the basin, while others favour high-density material below the Moho to be responsible for the very large subsidence and sediment accumulation (Artyushkov 2005).

(iv) The Post-Caledonian rift basins in the western Barents Sea exhibit smaller dimensions compared to the large single trough in the east. The Late Paleozoic structural development followed probably older NE (Caledonian) and N (Innuitian/Svalbardian) striking compressional orogens which intersect in the south-western Barents Sea (Gudlaugsson *et al.* 1998). A 300 km wide and fan-shaped array of rift basins and intrabasinal highs (Fig. 1) developed mainly during Middle Carboniferous times. From the Late Carboniferous onwards the western Barents Sea experienced regional subsidence interrupted only by renewed Permian-Early Triassic rifting close to today's continent–ocean transition. Permian salt structures occur in the diapir fields of the Tromsø and Nordkapp Basins, as local dome structures or as thick and deeply buried pillows (Breivik *et al.* 1995). The Middle-Late Jurassic and Early Cretaceous rifting mainly followed the track of the earlier development (Faleide *et al.* 1993). During the latter rift phase some basins (e.g. Sørvestsnaget Basin) subsided more than 12 km. Between eastern Svalbard and Franz-Josef Land on and offshore investigations revealed Cretaceous sills and dykes throughout the sedimentary succession from the Carboniferous onwards. Grogan *et al.* (1998) related this magmatism to the early break-up phase of Eurasia-Laurentia which involved extension also at interior locations. Seafloor spreading in

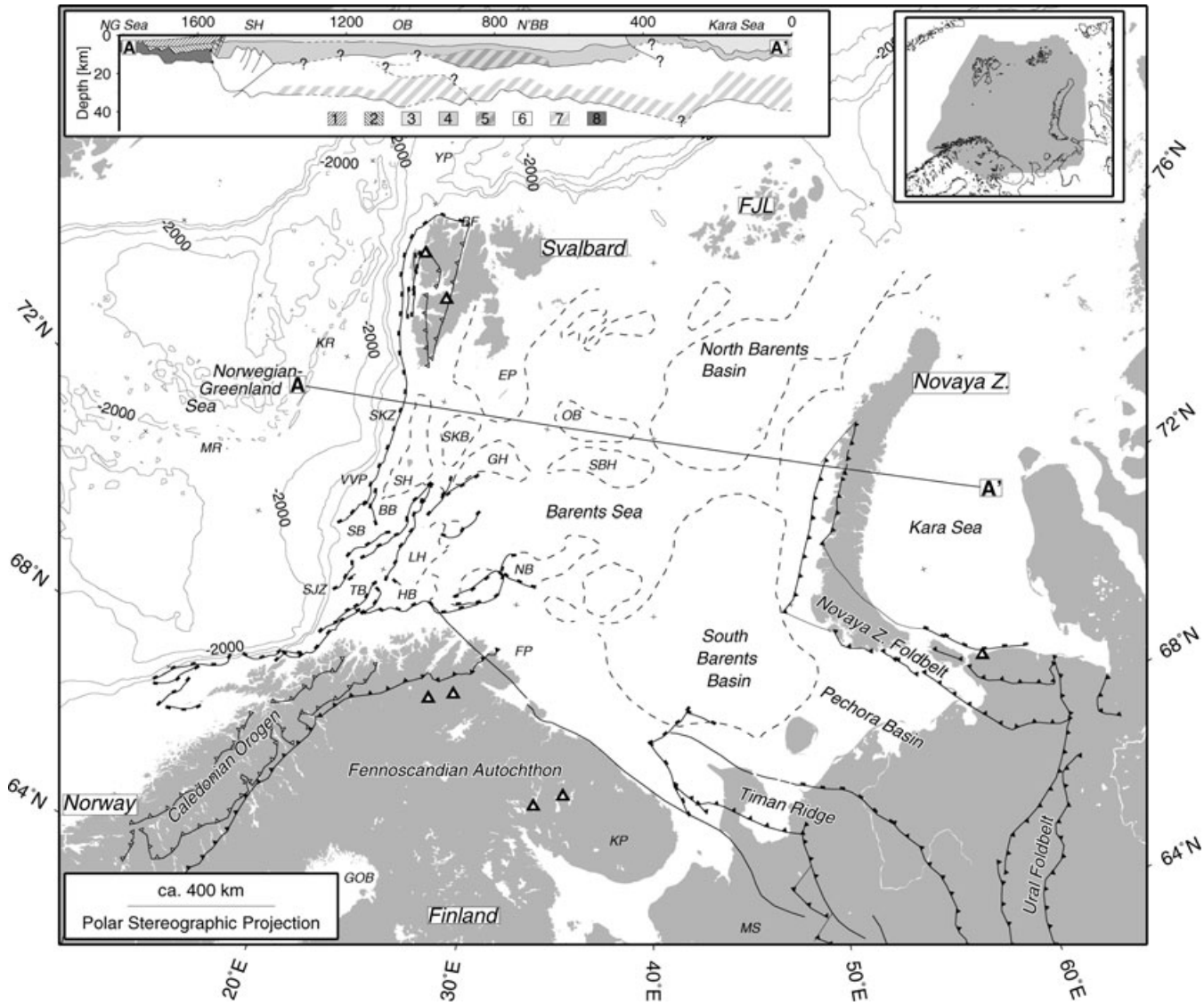

Figure 1. Overview map of the Barents Sea and surrounding regions. Open triangles mark the positions of permanent seismic stations. Dashed lines show prominent structural elements. Structures/places/names: BB, Bjørnøya Basin; BF, Billefjorden Fault; EP, Edgeøya Platform; FP, Finnmark Platform; FJL, Franz-Josef Land; GH, Gardabanken High; GOB, Gulf of Bothnia; HB, Hammerfest Basin; KP, Kola Peninsula; KR, Knipovich Ridge; LH, Loppa High; MR, Mohns Ridge; MS, Mezen Syncline; NB, Nordkapp Basin; OB, Olga Basin; SB, Sørvestnaget Basin; SBH, Sentralbanken High; SH, Stappen High; SKB, Sørkapp Basin; SKZ, Sørkapp Fault Zone; SJZ, Senja Fracture Zone; TB, Tromsø Basin; VVP, Vestbakken Volcanic Province; YP, Yermak Plateau. Bathymetry shown by grey 500, 1000, 2000, 3000 and 4000 m contours. Top insert (left) shows a geological profile from the Knipovich Ridge to the Kara Sea (A–A′). Patterns (in boxes): (1) Pleistocene Shelf Wedge; (2) Other Cenozoic sedimentary rocks; (3) Mesozoic sedimentary rocks; (4) Paleozoic sedimentary rocks; (5) Paleozoic sedimentary- and/or crystalline rocks; (6) continental crystalline rocks; (7) lower continental crystalline rocks ($v_p > 6.8\,\mathrm{km\,s^{-1}}$) and (8) oceanic crystalline rocks. Crust-cutting dashed lines in the western-central Barents Sea (km 800–1100) indicate a Caledonian main thrust. The transect was constructed on the basis of Johansen *et al.* (1993), Sigmond (2002), Breivik *et al.* (2002, 2003) and Sakoulina *et al.* (2003). The insert map on the top (right) shows the outline of the target region in grey.

the Norwegian-Greenland Sea and Eurasia Basins started in Early Eocene times. The spreading axis of the Mohns Ridge (Fig. 1) strikes nearly perpendicular to the western Barents Sea margin resulting in a sheared margin setting along the Senja Fracture Zone. Similarly, a second oceanic basin and a sheared margin developed southwest of Svalbard. The opening of the Norwegian-Greenland Sea was accompanied by extrusive magmatism in the Vestbakken Volcanic Province between the sheared margin segments (Faleide *et al.* 1991).

(v) The Pai-Khoi-Novaya Zemlya Foldbelt is located in the northern continuation of the Uralian Foldbelt between the East-European Platform (and the Fennoscandian autochthon) and the Siberian Platform. Collision started in late Devonian times in the southern and middle Uralian Foldbelt. The collision front propagated northward into the target region in Permian times. Between the Early and Late Jurassic the Novaya Zemlya Foldbelt developed (Puchkov 1996).

1.4 Previous crustal models

The Barents Sea region has been covered by different published crustal velocity models at various scales, based on different construction methods. In the following, we present a selection of earlier models since these will be compared with the model developed in the present paper.

Mooney *et al.* (1998) published the global crustal model CRUST 5.1 based on a compilation of first-order data, that is, mostly seismic refraction experiments. Only northern Scandinavia and parts of the Kola Peninsula were constrained by 1-D velocity profiles. Mooney *et al.*'s basic strategy was the generalization of the measurements into a limited number of crustal types with a defined velocity–depth structure. A primary crustal type was then assigned to each $5^\circ \times 5^\circ$ sized tile using *a priori* information such as the geological setting and, for continents, an average basement age. Our target region is represented in CRUST5.1 as a combination of cratonic provinces of Proterozoic age and provinces with extended continental crust (e.g. shelf regions, continental margins). Bassin *et al.* (2000) updated this global model (CRUST2.0) with a better fit to shelves and coastlines, ice thickness adjustments and a better sediment thickness model.

The WENA1.0 model was released by Pasyanos *et al.* (2004). Their approach was based on regionalization, that is, the subdivision into smaller geological units. The Barents Sea is, therefore, classified as continental shelf assuming a 32 km thick standard model. The Novaya Zemlya region is represented by the Uralian Foldbelt (48 km thick crust), while the southern onshore areas of Scandinavia are included in the Baltic Shield (45 km). The WENA1.0-model was sampled on a 1°-grid although the geophysical models for the crystalline crust were taken from Mooney *et al.* (1998), which was sampled at 5° and based on very limited information in the Barents Sea region.

The global model 3SMAC by Nataf & Ricard (1996) is based on a different approach: It compiled the basic chemistry of sedimentary, crystalline crustal and mantle rocks. Temperature and pressure in the crust and upper mantle, which control the local mineralogy, were inferred by thermodynamic modelling. From this they were able to deduce seismic velocities and densities.

The new 3-D velocity model developed here may also replace the simple crustal velocity models of Kremenetskaya *et al.* (2001) and Schweitzer & Kennett (2002) derived from regional seismological analysis in the European Arctic. These models are mainly averages of various local models and, therefore, do not account for the geological diversity found in the Barents Sea region.

2 VELOCITY DATABASE

The compiled database is based on different types of experiments. First, we acquired velocity models from seismic refraction experiments. Secondly, deep seismic reflection data in the western Barents Sea were used for density modelling which helped to infer the Moho depths along the profiles where the crust–mantle transition was not visible (transparent crust, no Moho reflection). The final density models were subsequently converted into velocity models. In combination with the models obtained from refraction experiments we increased the total number of 1-D seismic profiles from 570 to a total of 680 profiles.

2.1 Crustal velocity models from seismic refraction experiments

These profiles are mostly obtained from continuous 2-D profiles. Other models are based on localized marine expanded spread profiles (ESP), surface wave analyses or on simple non-reversed seismic lines, such as sonobuoy experiments. All continuous 2-D profiles were sampled every 25 km to generate simple 1-D velocity–depth profiles. This interval was chosen to map sufficiently well all relevant geological structures while at the same time avoid oversampling. Table 1 gives the sources of all seismic refraction studies and Fig. 2 shows the locations of all sampled 1-D velocity profiles entered into the database.

2.2 Crustal velocity models derived from deep seismic reflection data

Fig. 3 shows the deep seismic reflection profiles (IKU) in the western Barents Sea (Gudlaugsson *et al.* 1987). Locally, the crust–mantle transition is documented by strong lower crustal reflectivity or a clear Moho reflection (e.g. Fig. 4; IKU-B, km 400–500). On the other hand, large sections are characterized by transparent subsedimentary crust (e.g. IKU-B; km 225–375). To obtain the complete Moho relief, 2-D density modelling for each of the IKU profiles was carried out which focussed on the crust–mantle density contrast. Once a good fit to the observed gravity anomalies was achieved, the density structure was converted (back) to seismic velocities. As was done for the seismic refraction profiles the final models were sampled every 25 km (Fig. 2). Figs 4a and b show two representative examples of the modelling results for the profiles IKU-A and IKU-B.

2.2.1 ESP velocity data

The line drawing interpretations of the time sections were depth-converted using ESP (interval) velocity data. These data were taken from Jackson *et al.* (1990) and Sanner (1995). Some of the profiles' CMPs (common mid points) are not in-line with the IKU profiles and so, the CMP-locations were projected onto the profiles. To carry out the depth-conversion the 1-D seismic velocity profiles were linearly interpolated along each profile to a 2-D grid. Some structures were not well covered by nearby ESP data. In such cases, nearby 1-D velocity profiles were duplicated and adjusted using the seismic reflection data (e.g. shifting the sediment-basement interface).

2.2.2 Assigned densities

Major sedimentary sequences were picked from the converted sections following the stratigraphy shown in Table 2. Velocity–density relationships of sedimentary units in the western Barents Sea were obtained from the seismic refraction/gravity studies of Breivik *et al.* (1995); Breivik *et al.* (1998, 2002, 2003, 2005) and Mjelde *et al.* (2002). These profiles show a lower crustal boundary and are, therefore, in agreement with the locally observed reflectivity along the IKU profiles, although transparent crystalline crust was also modelled as two-layered crust. Densities of the upper- and lower-crystalline continental crust ($2720/2930\ \mathrm{kg\,m^{-3}}$) were calculated from 6.40 and 6.80 $\mathrm{km\,s^{-1}}$ (Breivik *et al.* 2002) using the velocity–density relationship of Christensen & Mooney (1995). During the gravity modelling no adjustments were made in sedimentary layers, with the exception of the very deep basins in the southwest of the IKU profile pattern (e.g. Bjørnøya Basin; Fig. 4b). Here, elevated densities were assumed to account for higher compaction compared to shallower occurrences of the same layer (e.g. $+70\ \mathrm{kg\,m^{-3}}$ for Lower Triassic to $+350\ \mathrm{kg\,m^{-3}}$ for Cretaceous). The lower crustal rocks of the Finnmark Platform were modelled with a slightly decreased density ($2720\ \mathrm{kg\,m^{-3}}$) to obtain a fit to the long wavelengths over the platform area. In contrast, the lower crust below some prominent highs in the west (e.g. Loppa High) exhibits a higher density of 2980 or $3050\ \mathrm{kg\,m^{-3}}$ which is supported by high velocity bodies seen in seismic profiles of Mjelde *et al.* (2002).

Table 1. Database references, number of profiles and data classes.

References	#Profiles	Control parameters	Class	Symbol (Fig. 2)
Breivik *et al.* (2002)	41	8	A	■
Breivik *et al.* (2003)	14	8	A	■
Breivik *et al.* (2005)	27	9	A	■
Ljones *et al.* (2004)	13	7	B	■
Mjelde *et al.* (2002)	13	7	B	■
Geissler (2001)	4	1	D	■
Ritzmann (2003)	14	6	B	■
Ritzmann *et al.* (2002)	14	7	B	■
Ritzmann & Jokat (2003)	11	7	B	■
Ritzmann *et al.* (2004)	14	7	B	■
This study	118	7	B	□
Sakoulina *et al.* (2003)	85	4	C	▼
Sellevoll (1983)	7	4	C	●
Helminsen (2002)	11	1	D	◉
Høgden (1999)	14	1	D	○
Verba *et al.* (1992)	45	1	D	▽
Guggisberg *et al.* (1991)	22	1	D	⋆
Walther & Flueh (1993)	15	1	D	◊
Neprochnov *et al.* (2000)	17	2	D	▲
Neprochnov *et al.* (2000)	16	2	D	▲
Mjelde *et al.* (1992), 1996	35	6	B	⋆
Kodaira *et al.* (1995)	7	4	C	☆
Jackson (2002)	70	2	D	▽
Bogolepov *et al.* (1990)	18	0	D	△
Kostyuchenko *et al.* (1999)	14	2	D	△
Jackson *et al.* (1990); Sanner (1995)	13	3	D	◇
McCowan *et al.* (1978)	1	1	D	♦
A. Egorkin (personal communication 1985)	9	2	D	♦
Egorkin (1991)	2	2	D	♦
Vol'vovskiy & Vol'vovskiy (1975)	5	2	D	♦
Kanestrøm (1971)	1	2	D	♦
Pentilla (1971)	1	2	D	♦
Azbel *et al.* (1989)	1	2	D	♦
Egorkin (personal communication 1990)	1	2	D	♦

2.2.3 Final match and density-to-velocity conversion

Figs 4(a) and (b) (upper graphs) show that about 80 per cent of the observed and calculated gravity is within an uncertainty range of ±5 MGal (∼3 per cent of the maximum range of the input data). Along the profiles IKU-E to H a match of *ca*. 95 per cent is achieved. Larger deviations between modelled and observed gravity of up to 20 mGal are observed along the profiles IKU-A, B and C at the continent–ocean transition. Studies demonstrated the importance of density variations in the upper mantle below the Norwegian-Greenland Sea (Breivik *et al.* 1999), but their exact shape and magnitude is difficult to assess (conf. surface wave inversion model of Levshin *et al.* 2005). High-pass filtering of gravity data was not appropriate due to overlapping wavelengths with structures in the Barents Sea region (Asbjørn Breivik, personal communication, 2006). The positive deflection west of km 100 on profile IKU-A (Fig. 4a) is probably a temperature effect within the upper mantle, therefore, no 1-D velocity–depth profiles were sampled close to the continent–ocean transition zone and the Norwegian-Greenland Sea.

The final densities of sedimentary horizons were converted back to seismic velocities using the relationships of Table 2. Densities for crystalline rocks were converted by the non-linear relationship of Christensen & Mooney (1995), a depth-dependent relationship that incorporates mantle rocks for crust–mantle comparative studies.

2.3 Qualities of the compiled 1-D crustal velocity models

Fig. 5 shows the spatial distribution of compiled crustal seismic velocities. To provide an estimate of the quality of the compiled database entries, the source profiles were sorted into data classes from A (best) to D (least good; Table 1). The more quality control parameters are fulfilled the better is the final class of the input data. The quality control parameters were (i) a close receiver and shot spacing which provided a dense ray coverage during modelling, (ii) appropriate large seismic sources with low frequencies, (iii) information about uncertainties of layer boundaries and velocities, (iv) small uncertainties and (v) application of modern techniques for uncertainty estimation, (vi) independent confirmation of the structures such as by density modelling or from multi-channel seismic (MCS) data, (vii) an in-line geometry of the experimental setup and reverse shooting, (viii) sufficient documentation of the experiment location (coordinate lists, maps), (ix) modern processing and modelling procedures (joint inversion, tomographic analysis) and (x) access to original data to avoid digitizing of printed material. Due to a large number of more recent experiments (post 1992) nearly 50 per cent are category A or B and provide outstanding to good input data quality. Unfortunately, database entries of categories C and D are often located onshore (Scandinavia and Kola Peninsula) or are predominantly located in the eastern part of the region.

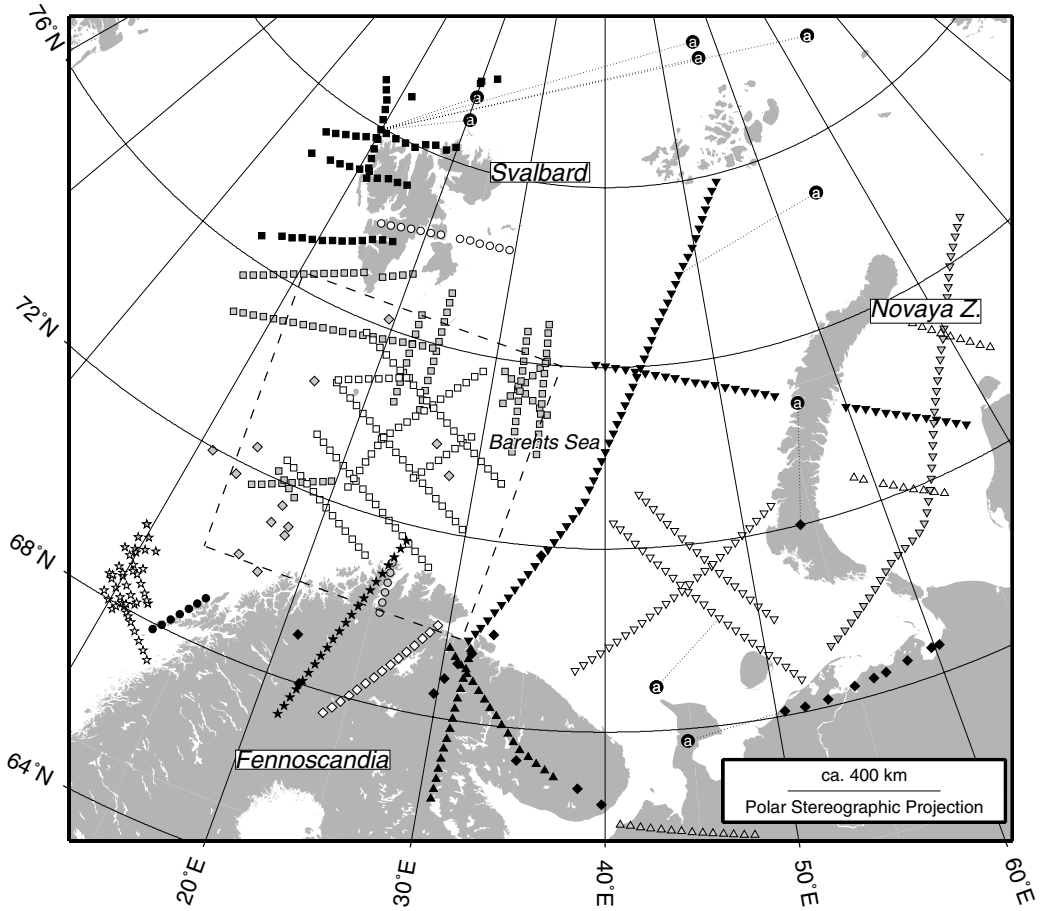

Figure 2. Location map of the seismic velocity–density database entries. See Table 1 for symbol codes and references. Black circles labelled with 'a' are duplicate database entries to constrain the velocity structure in regions where data coverage is poor. The dotted box gives the outline of the map shown in Fig. 3.

A detailed discussion of the uncertainties of the depths and seismic velocities of the layers in published models are, unfortunately, provided only more recently. Uncertainties for *P*-wave velocities and depths of shallow sediments are in the range of ± 0.10 km s^{-1} and ± 0.2–0.5 km, respectively. The velocity uncertainty range increases to ± 0.20 km s^{-1} if a non-reversed experimental setup or low energy seismic sources were used. Deeper sedimentary rocks with higher seismic velocities have larger uncertainties of ± 0.1–0.2 km s^{-1} (velocity) and 0.5–1.0 km (depth). The uncertainty range for some sedimentary layers is as high as ± 0.30–0.40 km s^{-1}, but this is not common.

The determination of seismic velocities of crystalline crustal rocks is more difficult with increasing depth. Low velocity gradients and increasing recording distances for waves penetrating the middle and lower crust entail a rapid decrease of the signal strengths. Therefore, the uncertainty boundaries increase from *ca*. ± 0.04–0.20 km s^{-1} in the upper and middle crystalline crust to ± 0.10–0.25 km s^{-1} in the lower parts. Often, the lowermost crust is not constrained by first arrivals. Instead, the move out and the amplitude strengths of Moho reflections were used to infer the seismic velocity above the crust–mantle boundary. Uncertainty ranges are, therefore, between 0.20 and 0.40 km s^{-1}. Uncertainties of depths of crystalline crustal horizons lie between 0.5 and 1.5 km. Due to strong reflections at the Moho compared to only weak reflections at middle crustal level, the depth uncertainty of the Moho is often better than the uncertainties with the crust.

To obtain an uncertainty for the density modelling results of the IKU profiles, a crossover analysis was carried out. The maximum difference in the depth of sediment horizons was ± 0.20 km (± 0.50 below 10 km depth). The mismatch between Moho depths did not exceed 1.0–2.0 km, which is in accordance with typical uncertainties found in seismic refraction models. A local exception is given between IKU-C and profile A of Mjelde *et al.* (2002) with a large mismatch of 6 km.

2.4 Unconstrained regions

To strengthen the interpolation additional nodes were included where the data coverage was weaker. To this end, 1-D velocity models were duplicated within the northern continent–ocean transition (Fig. 2), where 1-D profiles from the northern Svalbard margin region were inserted in the east. Moreover, the northern part of the Novaya Zemlya Fold Belt is poorly covered; here, a model was duplicated to the north. Finally, the structures of the northern East Barents Sea Basin and Pechora Basins were constrained by two additional profiles on their outer margins.

3 VELOCITY MODEL COMPILATION

3.1 Geological provinces

To maintain local characteristics of the different geological units in the model region, the model compilation is based on defined

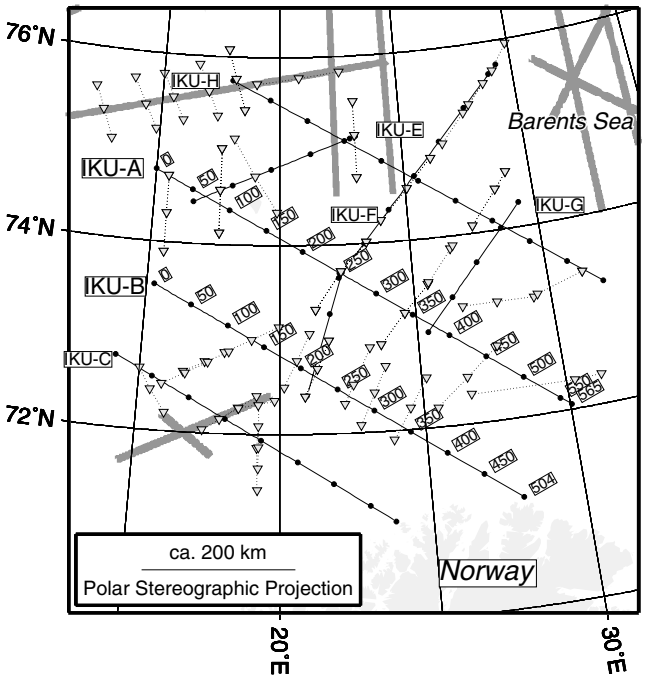

Figure 3. Locations of the IKU profiles A to H. Black dots mark 50-km sections along the profiles. Inverted triangles and connecting dotted lines indicate the positions of selected ESPs. The IKU profiles are also shown in Fig. 2 as open squares. ESPs not used for the depth-conversion of the line drawings are included in the velocity database and shown as grey diamonds in Fig. 2. Thick grey lines indicate seismic refraction profiles used for crossover analysis.

provinces (Fig. 6a). These provinces share a similar tectonic, sedimentary and magmatic history, they occur in various sizes, and were defined from surface constraints, such as faults and lineaments. The primary divisions are the separation of onshore from offshore areas and oceanic from continental domains. Onshore Fennoscandia, the Caledonides in the west adjoin the Fennoscandian Shield (Mosar *et al.* 2002). The continent–ocean boundary was obtained from Engen (2005) and the Permo-Triassic convergent zone of the Novaya Zemlya Fold Belt was outlined according to Bogatsky *et al.* (1996). Two provinces have younger magmatic histories. First, Cretaceous magmatism could have resulted in underplating between Svalbard and Franz-Josef Land (Grogan *et al.* 1998). Secondly, volcanic rocks were extruded in the Vestbakken volcanic province in Eocene times (Faleide *et al.* 1993). Their province boundaries were obtained from MCS data interpretations and integrated studies. Sedimentary basins and structural highs in the Barents Sea are based on Johansen *et al.* (1993).

Lithosphere is 3-D and suture zones between basement provinces or micro continents may have low dips so that 1-D velocity profile in the database may sample different provinces with depth. We estimate the number of profiles sampling different provinces to only a few, due to the lateral sampling interval of 25 km along continuous transects and 50 km of the final velocity model. However, we observed regional linear relationships between the sediment thickness and the thickness of the crystalline crust which support the idea of working with subregions (Fig. 7; see also Section 5.1). Since we compiled an area-wide sediment thickness map (Fig. 8) these relations can be used to adjust the thickness of the crystalline crust after compiling an interpolated velocity model. We favour this compilation method, since secondary constraints (i.e. the thickness relations) help to infer a better crustal thickness, which is one critical parameter for seismological event location. On the other hand, working with geological provinces results in fixed boundaries which are naturally much smoother. Geological interpretations will, therefore, be hardly reasonable at province boundaries.

3.2 3-D Velocity model format

The aim of this study was to construct a 3-D geophysical model with a higher resolution than provided by earlier published models which have a minimum node spacing of at least two longitudinal and latitudinal degrees. The model region extends from 66°N to 83°N, hence one degree of longitude reduces from *ca*. 45–13 km. With respect to the distribution of velocity data (Fig. 2), a model defined by longitudes and latitudes would result in an increasing number of nodes towards the north, in parallel with decreasing database constraints. The final model node spacing is, therefore, 50 km (Fig. 6b) and every non-marginal node has six neighbours. The final model is built on a total of 1490 nodes. Every node is defined by a velocity structure with up to two sedimentary layers and up to three crystalline crustal layers. The velocity between the upper and lower sediments is 3.0 km s^{-1}. The velocity boundaries between the three crystalline crustal layers are dependent on the tectonic setting. The boundaries and their values are provided in Table 3 and Fig. 5. We kept the number of different velocity boundaries as low as possible to allow comparability. Most regions in the Barents/Kara Sea share similar velocity boundaries (Figs 5d and e). Here, the velocity boundaries were chosen to maintain the predominant two-layered structure (e.g. Breivik *et al.* 2003; Sakoulina *et al.* 2003; Ritzmann *et al.* 2004) with local high velocity bodies in the lower crust.

3.3 Compilation of the preliminary model

Seismic velocity and thickness grids were calculated for each of the five model layers (two sedimentary layers and three crystalline crustal layers) independently for each geological province. If the database profiles contained more than one layer for a model layer, we added up their thicknesses and averaged their velocities. Velocities and layer thicknesses were interpolated using a continuous curvature gridding algorithm (Smith & Wessel 1990). The minimum and maximum of the calculated grids were limited by the input data. Subsequently, the thicknesses and velocities were sampled at the model node locations of the 3-D model (Fig. 6b) and compiled into 1-D velocity–depth profiles. Sedimentary layers thinner than 0.05 km and crystalline crustal layers thinner than 0.2 km were omitted, corresponding to the resolution of most of the included seismic refraction studies. A mean water depth or land height was assigned to each preliminary 1-D velocity profiles using the average levels of the surrounding topography.

Due to a strong tension factor applied during the curvature gridding (0.9) the resultant mean errors and the rms-misfits of the grids to the original data are very low. In most cases, the mean errors are within 2 per cent of the maximum input value. The rms misfits are, therefore, as low as 0.1 km for layer thickness grids and 0.01 km s^{-1} for layer velocity grids, respectively. Only ten of 270 grids have larger mean errors between 2 and 4.6 per cent of the maximum input value. Therefore, we concluded that the gridding algorithm was generally applicable.

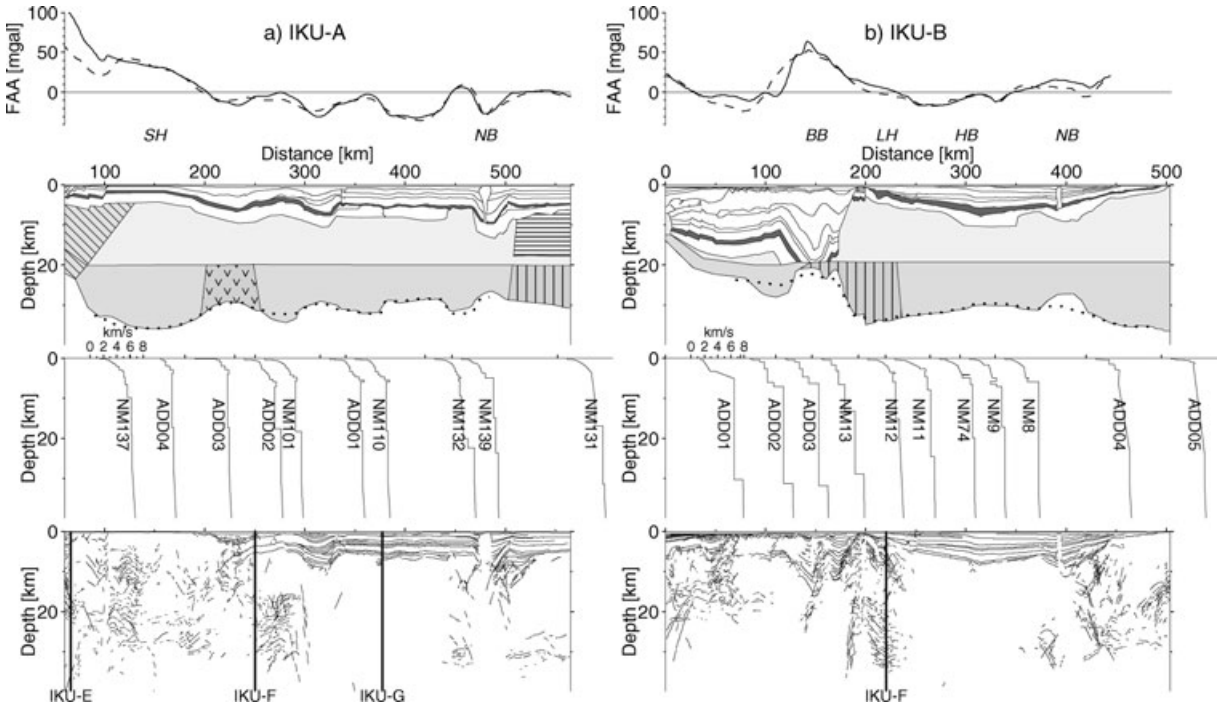

Figure 4. Line drawings (depth sections), 1-D velocity functions, density models and resultant gravity profile (bottom-up) along profiles IKU-A and B. IKU cross-profiles are indicated by thick vertical lines. Second panel from the bottom shows seismic velocity function from ESPs used for depth-conversion of the line drawing. For a horizontal (velocity) scale see left graph in panel. Functions labeled as ADD are derived from neighboring ESP data (NM) to account for local structures. The final density models are shown third from the bottom. Sedimentary layers are coloured in white, with exception of the Permian (2640 kg m^{-3}, dark grey, other densities see Table 2). Modelled density anomalies of crystalline rocks are indicated by the following patterns: horizontal, 2700 kg m^{-3}; vertical, 2980 kg m^{-3}; v-pattern, 3050 kg m^{-3}; diagonal, 2720 and 2820 kg m^{-3}. The Airy-compensated Moho depth is shown by a dotted line. Upper graphs show the comparison between observed (dashed) and modelled (solid) free-air gravity anomaly.

Table 2. Sedimentary layer mean densities in the western Barents Sea.

Layer	Density (kg m^{-3})	*P*-wave velocity (km s^{-1})
Quarternary	1800	1.80
Tertiary I	2050	2.25
Tertiary II	2280	3.26
Cretaceous I	2240	2.75–3.60
Cretaceous II	2370	
Cretaceous II	2590	
Upper Triassic I	2380	4.00–5.45
Upper Triassic II	2590	
Middle Triassic I	2470	
Middle Triassic II	2590	
Lower Triassic I	2520	
Lower Triassic II	2590	
Permian	2640	4.50–5.90
Pre-Permian	2710	5.50–6.00

3.4 Layer thickness adjustments

The preliminary model compiled in the previous step was then adjusted where no constraints from 1-D velocity profiles existed. If a 1-D velocity profile of the database constrained the model node within a radius of 25 km, the thicknesses were not altered. On the other hand, if no database entry was found nearby, the sediment and crystalline crustal thicknesses were determined by area-wide sediment thickness data (Fig. 8) and the regional thickness relationships (Fig. 7). These adjustments were not possible for provinces overprinted by convergent tectonics, where the sediment thickness is locally altered due to uplift and erosion (Caledonian Foldbelt, Pai-Khoi-Novaya Zemlya Foldbelt), sediment-free cratons (Fennoscandia) or oceanic crustal domains, where the crystalline crustal thickness is predominantly a function of the asthenosphere temperature at the spreading ridge. Nevertheless, about half of the nodes (729) could be adjusted using these second-order (geological) constraints.

The thickness adjustments for the 1-D velocity models were performed as follows: (i) The sediment thickness on a 1-D profile was compared to the sediment thickness compilation. (ii) If the thickness deviates more than 5 per cent and no velocity database entry was found within a radius of 25 km, the thickness of sediment layers of the 1-D profile was adjusted according to the sediment thickness map, that is, thinned or thickened proportionally (e.g. upper/lower sediments with 1/5 km thickness were adjusted to 1.5/7.5 km if the sediment thickness map shows 9 km total thickness). (iii) The thickness of the crystalline crust was calculated using the regression parameters of this province (Fig. 7) and compared to the thickness of the crystalline crustal layers of the preliminary 1-D model. If no nearby data constraints were given the crystalline layers were adjusted proportionally to the calculated total thickness.

The sediment thickness map we used (Fig. 8) is based on the depth-to-basement compilations of Myklebust (1994), Engen (2005) and Bogatsky *et al.* (1996). These studies were based on MCS data and shallow seismic refraction data. Further, seismic data were interpreted along with gravity and magnetic field anomalies, and compared with the geological record. Sedimentary thicknesses on Franz-Josef Land are largely unknown. About 6 km of Pre-Quaternary deposits have been mapped from onshore outcrops and about 4.8 km are drilled (Dibner 1998); deep seismic data

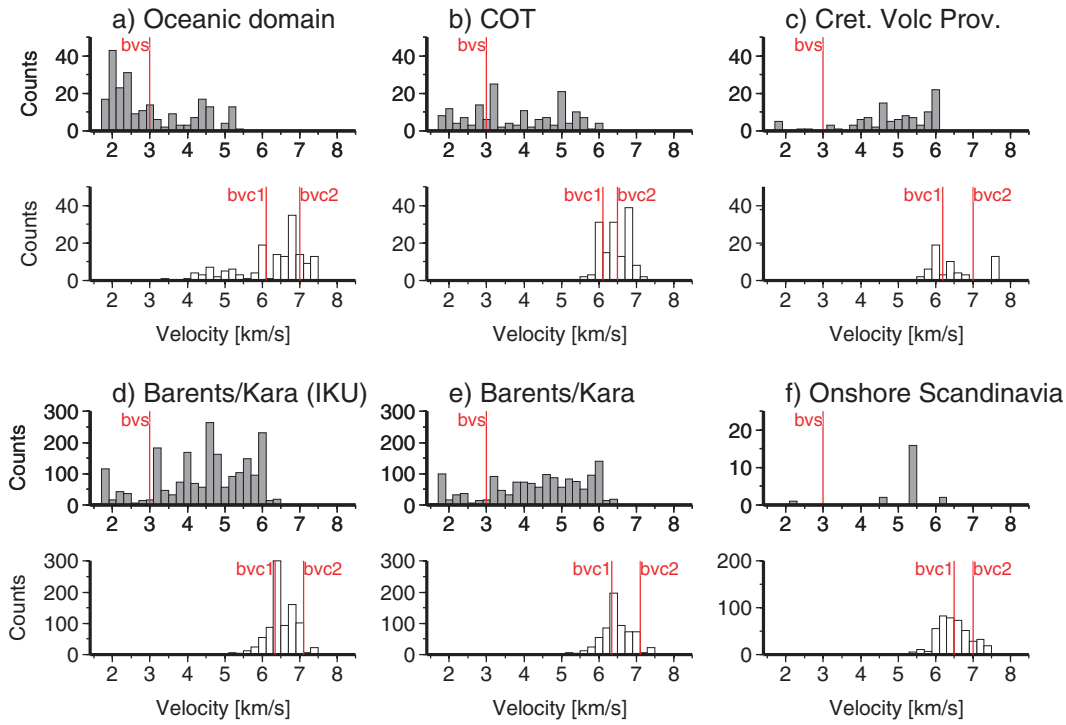

Figure 5. Histograms showing the observed *P*-wave velocities in the study region. Grey bars (upper) and white bars (lower) show seismic velocities for sedimentary rocks and crystalline rocks, respectively. (a) Provinces with oceanic crust. (b) Continent–ocean transition zones in the west in north of the model. (c) The Cretaceous Volcanic province. (d) The remaining areas of the Barents and Kara Seas with data converted from density modelling. (e) Same as (d), but without the data converted from density modelling. (f) Caledonian- and Precambrian autochthon provinces of onshore Fennoscandia. Red vertical lines within the histograms indicate the velocity boundaries chosen for the different provinces. bvs, boundary velocity sediments; bvc1, boundary velocity between upper- and middle-crystalline crust; bvc2, boundary velocity between middle and lower crystalline crust. See also Table 3. Note, the different vertical scales.

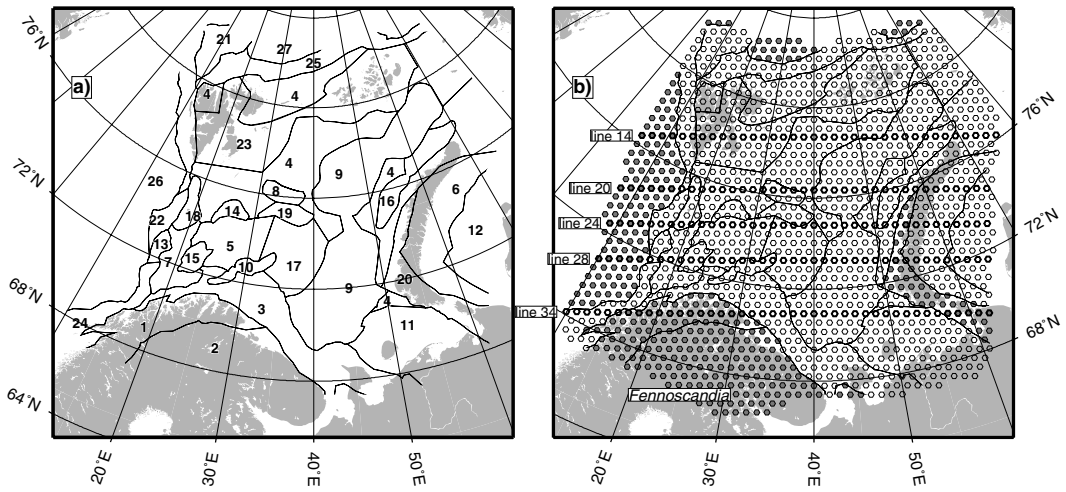

Figure 6. Geological provinces and grid node setup. (a) Geological provinces in the target region: (1) Caledonian Foldbelt; (2) Fennoscandia (Authochthon); (3) Finnmark Platform; (4) General Platform; (5) Bjarmeland Platform; (6) Novaya Zemlya Microplate; (7) SW' Sedimentary Basins; (8) Olga Basin; (9) East-Barents Sea Basin; (10) Nordkapp Basin; (11) Pechora Basin; (12) South Kara Basin; (13) Sørvestsnaget Basin; (14) Gardabanken High; (15) Loppa High; (16) NW' Novaya Zemlya Highs; (17) Central Barents High; (18) Stappen High; (19) Sentralbanken High; (20) Novaya Zemlya Foldbelt; (21) Yermak Plateau; (22) Vestbakken Volcanic Province; (23) Cretaceous Volcanic Province; (24) Western continent–ocean transition; (25) Northern continent–ocean transition; (26) Norwegian Greenland Sea; (27) Nansen Basin. (b) Grid nodes of the BARENTS50 model. Gray-shaded nodes are located in oceanic provinces, provinces overprinted by convergent tectonics and sediment-free cratons. Bold hexagons give the location of the transects shown in Fig. 12.

indicate thicknesses up to 12 km, while estimations from gravity data indicate about 8–9 km. For Franz-Josef Land and the north-eastern corner of the model region, a sediment thickness of 8 km was chosen to complete the compilation. Towards the north, the thickness was set to 5 km to account for uplift and erosion during the initial rifting of the Eurasian Basin (Dimakis *et al.* 1998). The sediment thickness map was corrected using the depths of our newly compiled database. Basement depths of the database entries

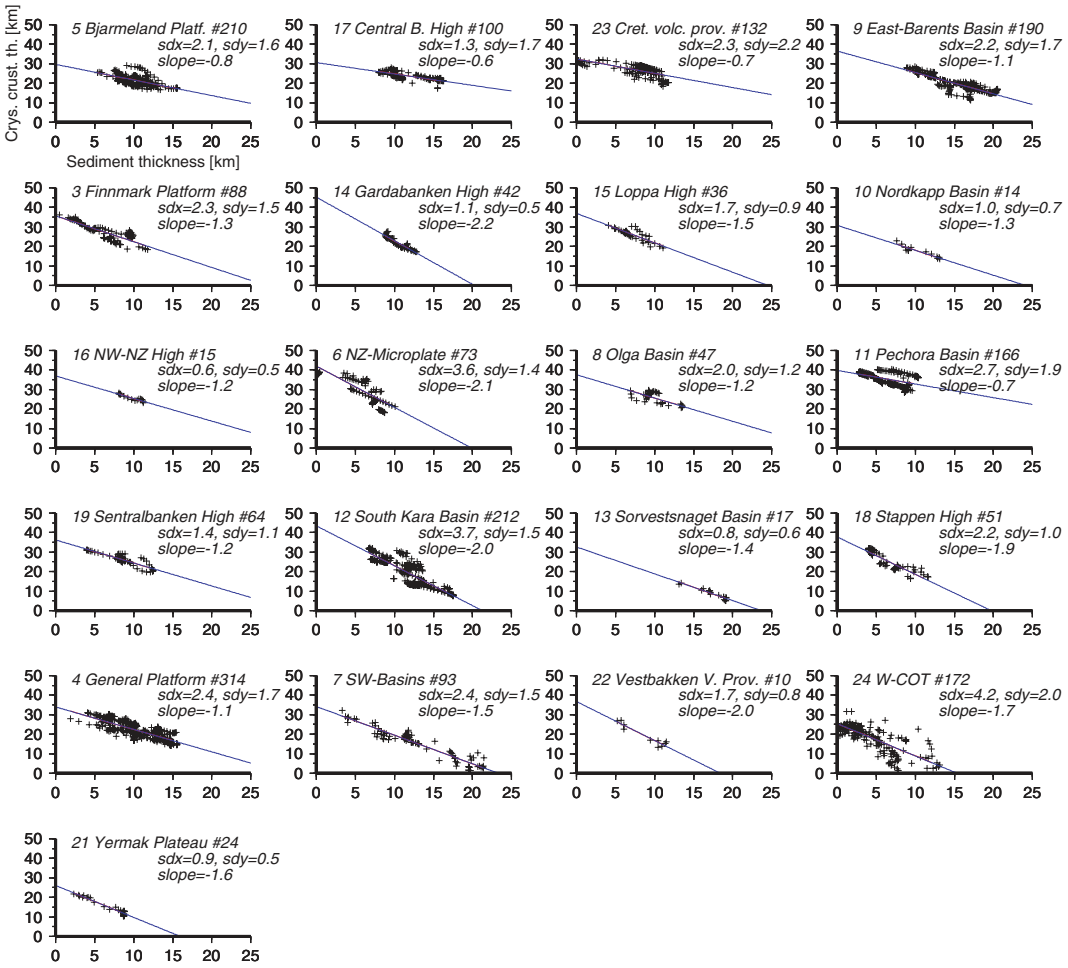

Figure 7. Sediment thickness plotted against crystalline crustal thickness for all provinces (excluding sediment-free cratons, oceanic crustal domains and regions overprinted by convergent tectonics). Black crosses are datapoints extracted from the profile database. The solid lines show the calculated linear regressions. The total number of observations is given after the #-sign. The sdx and sdy values give the standard deviations of the sediment thickness and crystalline crustal thickness, respectively.

were compared with the sediment thickness map and, in the case of mismatch, used for adjusting the sediment thickness map.

3.5 *S*-wave model

After the compilation of the *P*-wave velocity model, the BARENTS50 model was extended by including *S*-wave velocities for every crustal layer. Average V_p/V_s ratios for the crustal layers were extracted from the lithosphere model of Levshin *et al.* (2005) and used for the conversion of the *P*-wave velocities in our model. The mean V_p/V_s ratios for the upper- and lower-sedimentary layer are 3.01 and 1.73, respectively. Below, the three crystalline crustal layers exhibit ratios of 1.70, 1.72 and 1.75, respectively.

3.6 Uncertainty of the velocity model

The lower bound uncertainties for the seismic velocities of the 3-D model are constrained by the quality of the input velocity data. As discussed earlier, not all of the included studies provide a detailed discussion of the final velocity model uncertainties. However, a minimum estimate can be taken from the discussion of model qualities above (Section 2.3). The algorithm used to grid velocity and layer thickness forced strong tension (Smith & Wessel 1990) to maintain the data input as well as possible in the calculated model. Seismic velocity uncertainties at nodes with no nearby data constraints are difficult to estimate. In general, the applied algorithm allows interpolated values only within the input range. If model nodes are constrained by more than one model, these were averaged and a mean was used for gridding. The range of seismic velocities of the input models is described by the standard deviations of the individual layer velocities which are lower in the upper sediments and middle and lower crystalline crustal layers ($\sigma = 0.38$, 0.24 and 0.22 km s^{-1}, respectively). The input velocity range is significantly higher in lower sediments and upper- crystalline crust ($\sigma = 0.88$ and 0.73 km s^{-1}). However, this does not describe the actual uncertainty of single calculated velocities.

An uncertainty estimate for the layer depths of the model can be inferred from the scatter of the relationship between the sedimentary and the crystalline crustal thickness of the geological provinces. The standard deviations of the regressions provide the thickness uncertainty with respect to the regression model. The total sedimentary layer thicknesses have σ-values between 0.5 km (Yermak Plateau) and 1.7 km (East Barents Sea Basin). Provinces characterized by significantly higher scatter show deviations up to 2.2 km (western continent–ocean transition), corresponding to 20 per cent of the

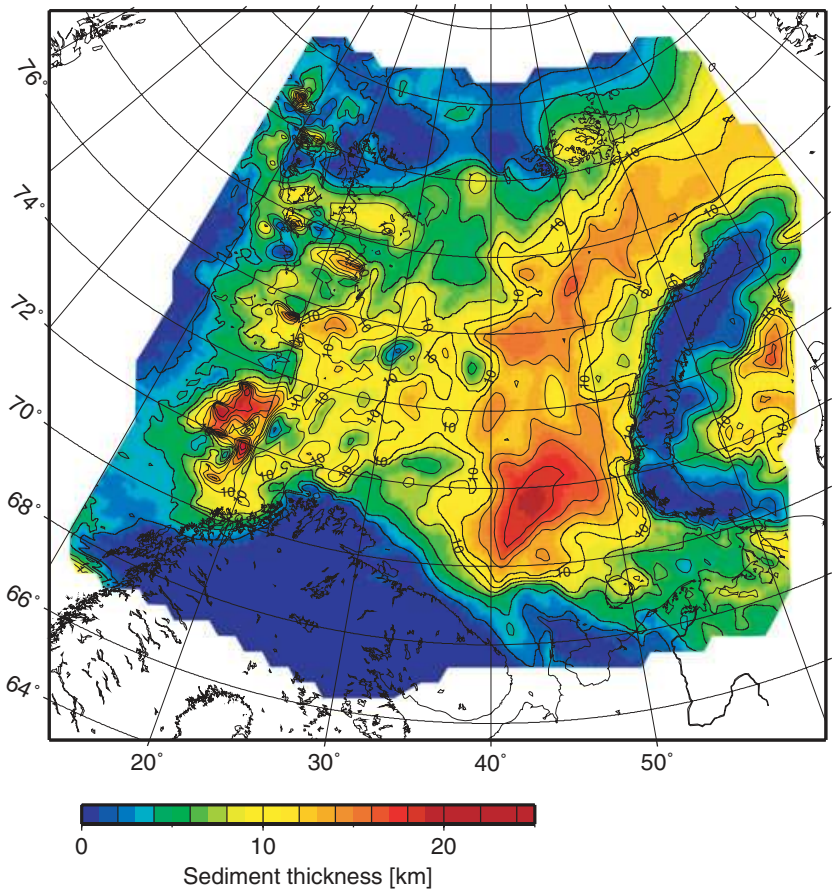

Figure 8. Sediment thickness map used for layer thickness adjustments of the preliminary model where no nearby data constraints (1-D velocity profiles) were given.

Table 3. Velocity boundaries between the three crystalline crustal layers.

Tectonic setting	Velocity boundary upper-middle/ middle-lower crust (bvc1/bvc2) (km s^{-1})
Barents Sea	6.4/7.1
Oceanic provinces	6.1/7.0
Continent–ocean transitions	6.1/6.5
Cretaceous volcanic province	6.2/7.0
Onshore Scandinavia	6.5/7.0

total sedimentary thicknesses. Uncertainties in the thickness of the crystalline crust are higher and mostly >1 km, while more than the half of the provinces show values >2 km. At maximum, this is about 20 per cent of the total crystalline crustal thickness.

4 DENSITY MODEL COMPILATION

In addition to the seismic velocity structure we provide the 3-D crustal density structure. Our strategy was as follows: The velocity model was converted to a density model and used for gravity calculation. The obtained gravity field was subsequently compared to the observed gravity field and locally adjusted within a defined uncertainty range using a grid search method. With the exception of the western Barents Sea, where the velocity model was predominantly derived from density modelling (Fig. 4), this step was an independent test of the *P*-wave velocity model. We expected (at least) a minimum fit using standard relations between seismic velocity and density outside this area.

4.1 The observed gravity anomalies in the target region

Fig. 9(a) shows the observed free-air gravity anomalies in the target region from the Arctic Gravity Project (http://earth-info.nga.mil/GandG/wgs84/agp/). Prominent positive anomalies occur over onshore regions and seaward of the continent–ocean transitions, where locally more than 150 MGal are observed (e.g southwest of Svalbard). In the Barents Sea positive anomalies are significantly lower. Here, some of the prominent structures such as the Sentralbanken High show only 20 MGal. Some structures reveal an unexpected gravity field. Breivik *et al.* (2002) showed that the Olga Basin is characterized by a positive anomaly similar to the Sentralbanken High. Despite large geological contrasts in the Barents Sea, with deep sedimentary basins and local basement highs, the gravity field is generally very smooth. Negative anomalies are not lower than −40 MGal. Gravity anomalies in the western Barents Sea reveal shorter wavelengths compared to the east. The average gravity anomaly in the Kara Sea is slightly lower than in the eastern Barents Sea.

4.2 Gravity calculation

The gravity of a single body can be calculated using Plouff's (1976) derivation of the integral over the limits of a prism. The total gravity over the model nodes (Fig. 6a) was calculated by summing the

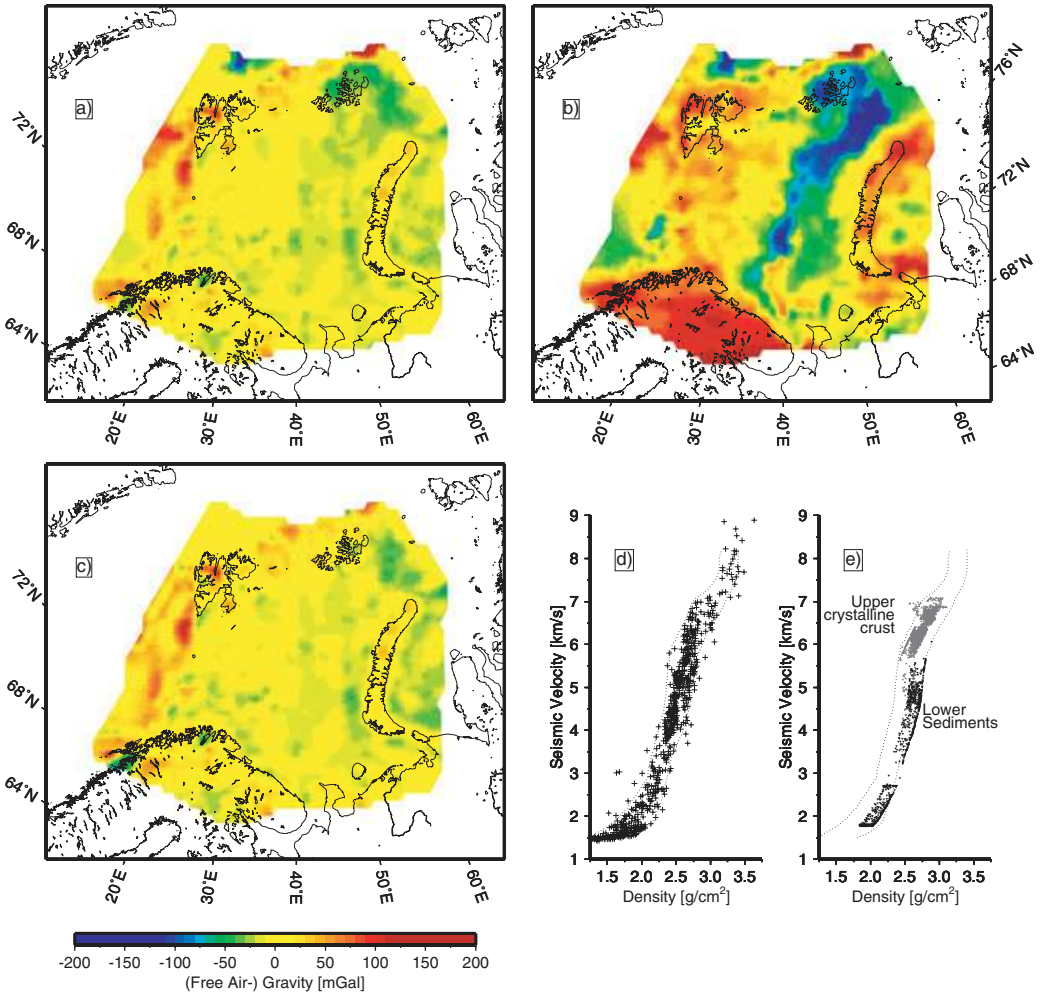

Figure 9. Gravity modelling. (a) Free-air gravity anomalies in the study region. (b) Gravity field, inferred from the initial density model. (c) Gravity field, inferred from the adjusted density model using grid search. (d) Relationship between seismic *P*-wave velocity and density from Ludwig *et al.* (1970). Dotted lines indicate the minimum and maximum density for each velocity after Barton (1986). (e) Adjusted densities using the grid search method of the lower sediments (black) and upper-crystalline crust (grey).

individual fields of the 50 km × 50 km wide prisms (layers) of the velocity profile. Up to five density-converted crustal layers and a mantle layer constitute the 1-D profile of the model. The water column was set to a value of 1030 kg m^{-3}. Sedimentary rock velocities were converted using the mean density value of the defined minima and maxima of Barton's (1986) review of velocity–density relationships (Fig. 9d). Crystalline continental rock velocities were converted by applying the depth-dependent relationship of Christensen & Mooney (1995) for crust–mantle studies. Densities of oceanic basaltic rocks were computed from Christensen & Smewing (1981), in which the density is related to the burial depth below the base of sedimentary rocks and the water column. Mantle rock densities were set to 3300 kg m^{-3}. Velocity–density relationships generally reveal a significant scatter (Fig. 9d) for any rock type. Later, we take advantage of this uncertainty range during the search for refined density values to obtain a better fit to the observed gravity.

4.3 Gravity field of the initial density model

Fig. 9(b) shows the gravity field inferred from the initial density model which was based on the velocity–density relationships introduced above. The striking difference, compared to the observed gravity field (Fig. 9a), is the difference between the western and eastern Barents Sea. The western half is characterized by positive anomalies, while the eastern half shows a very low gravity field (< -120 MGal) following the outline of the Eastern Barents Sea Basin. A similar low gravity field was calculated over the deep sedimentary basins in the south-western Barents Sea (e.g. Bjørnøya Basin). As discussed earlier, the seismic velocities of the model layers are average velocities. The total range of velocities in the upper sediments and middle and lower crystalline crustal layers is limited (i.e. 1.8–3.0, 6.2–7.1 and 6.6–7.6 km s^{-1}, respectively), while the range is significantly higher in lower sediments and upper-crystalline crust (i.e. 3.2–6.0 and 4.1–6.5, respectively). Sediments experience compaction while crystalline basement rocks in the upper-crust experience the closure of pores and cracks causing strong vertical velocity gradients. The most uncertain density contrast in the layered model is, therefore, at the sediment-basement boundary (in addition to the crust–mantle transition), since the model layers contain mean velocities. Densities calculated for the rocks directly above and below this boundary may deviate significantly from the real conditions. The calculated gravity field, therefore, reflects the basement relief, that is, regions with a thick sedimentary cover show very low gravity values.

4.4 Density grid search

Since the velocity–density relationships show a significant scatter a grid search algorithm was developed to obtain densities which provide a better fit to the observed gravity field. The grid search focussed on the density contrast between sedimentary cover and the crystalline crust, since the largest uncertainties are expected here. The density grid search limits were given by Barton (1986). Here, the scatter around the average density is between ± 200 and ± 300 kg m^{-3}. The densities of the sedimentary layers and upper-crystalline layers were increased or decreased in discrete steps of 10 kg m^{-3} according to the mismatch between the observed and calculated field at the grid node. After each iteration, the gravity field calculated from the model is compared to the observed field. We regarded the grid search as converged once the observed field was matched within a range of ± 5 MGal, since our investigation is focussed on regional crustal structures. If the uncertainty range of possible densities of sedimentary layers was exceeded the grid search was halted. The grid search resulted in a reduction of the density contrast between the lower sediments and the upper-crystalline crust. Fig. 9(e) illustrates the final density adjustments.

4.5 Gravity field of the adjusted model

After the grid search, the gravity inferred from the adjusted model matches the observed field very well in the Barents and Kara Seas and onshore regions (Fig. 9c). A large number of nodes match the observed field to within ± 5 MGal. The most prominent mismatches are the region of Franz-Josef Land and the Yermak Plateau, west of Svalbard, and off north-western Norway. As discussed earlier, the sediment thickness in the vicinity of Franz-Josef Land is not well constrained and the use of a regional average depth may contribute to the observed mismatch. The strong positive anomaly west of Svalbard occurs in the vicinity of the spreading ridge system, where upper-mantle densities may be lower than 3300 kg m^{-3}, either from serpentinization (Ritzmann *et al.* 2002) or the rising asthenosphere (Breivik *et al.* 1999). We therefore, conclude that the compiled *P*-wave velocity model is independently confirmed where seismic velocity constraints were not derived from density modelling (i.e. western Barents Sea). On the basis of standard relationships between seismic velocity and density and adjustments within the given uncertainty range we were able to fit the gravity field sufficiently well.

5 DISCUSSION

5.1 The limits of the province-dependent thickness relationships

A fundamental step during the velocity model compilation was adjusting the crustal thickness according to (linear) relationships between the sediment thickness and the thickness of the remaining crust as a function of geological provinces (Fig. 7). The most important assumption behind this approach is that subsidence and the development of sedimentary basins is coeval with the flexure and/or thinning of the underlying crust. Regional conditions, such as density of the crust and mantle, the strain and stress rates, the viscosity and strength of the crust and, obviously, the sediment supply result in a specific (local) thickness relation between the sedimentary cover and the remaining crust. Simple models of crustal extension (e.g. McKenzie 1978) show that after the cooling of the stretched lithosphere (>120 Ma) the relation between basin depth and the crystalline crustal thickness follows a straight line similar to an Airy-type isostatic compensation model (e.g. Watts 2001). Prior to the state of thermal equilibrium the ratio between basin depth (sediment thickness) and the thickness of the thinned crystalline crust is slightly curvilinear. If, for example, the density of the crust is increased, the straight lines get steeper slopes; similarly, we expect other regional parameters to contribute to the final trend of the relationship. The latest phase of rift-related subsidence and deposition was in the Early Cretaceous (100 Ma; Faleide *et al.* 1993).

Fig. 7 shows, despite the scatter, that most distribution patterns reveal trends which can satisfactorily be expressed through linear regressions. The standard deviations for the sediment (*x*-axis) and crystalline crustal thicknesses (*y*-axis) do not exceed 20 per cent of the observed thicknesses and are often considerably lower. The scatter is highest in the case of the continental margin in the western Barents Sea (Fig. 7; province 24) where the standard deviation is 4.2 at sediment thicknesses between 0 and 15 km. Fitting the data by linear regression in this province is problematic since rifting and break-up occurred in Late Cretaceous and Eocene times and the thermal subsidence is probably not completed. Other provinces show very low scatter such as the Nordkapp Basin (province 10) or the basement highs off NW Novaya Zemlya (province 16).

A large number of parameters, such as the incomplete filling of the accommodation space, compaction rates, inversion events or changing basement rock properties (e.g. density) can lead to large scatter or eventually to major errors in the interpretation of the linear relationships. The thickness adjustments made on the basis of these relationships are up to several kilometres. The crystalline crustal thicknesses of provinces which are characterized by very little scatter (e.g. 5, Central Barents High; 17, Cretaceous Volcanic Province; 23, East Barents Sea Basins; 9, Finnmark Platform) were locally adjusted up to 7 km, which exceeds the observed scatter. Fig. 10 emphasizes the importance of these adjustments. It shows the sediment thickness, the interpolated crustal thickness for the preliminary model and the adjusted crustal thickness for the example province of the Central Barents Sea High (Fig. 7, province 17). The sediment thickness (Fig. 10a) shows clear internal structuring between basement highs (6 km) and deeper sedimentary troughs (>14 km). The interpolated crustal thickness, however, does not reflect this structuring. The interpolation is guided by the constant crustal thickness of the profile in the north-west (35 km) and the crustal thickening of the profile in the east (35–40 km). The independently acquired crustal profiles of this province show a strong linear thickness relationship (Fig. 7; mostly from Breivik *et al.* 2002; Sakoulina *et al.* 2003). If this relationship also applies for the region between the two profiles remains open for debate, since we have no data constraints on the complex crustal properties here. We expect a degree of crustal thinning during sediment basin formation, and we account for this using the thickness adjustments shown in Fig. 10c. We conclude that the usage of the thickness relationships is only a simple approximation to a very complex interplay of regional tectonic history and a wide range of rock properties. We believe that this approximation provides a more likely and natural solution than the 'pure' mathematical solution.

Other 3-D models, however, evolve from gravity modelling based on isostatic and flexural principles (e.g. Kimbell *et al.* 2004). The degrees of freedom increase substantially when using potential field data, due to the lack of density information within unconstrained regions. A promising future solution may be the joined inversion of the gravity field and the thickness relationships. Here, also a more complex mantle density model (taken from surface wave data) can be incorporated.

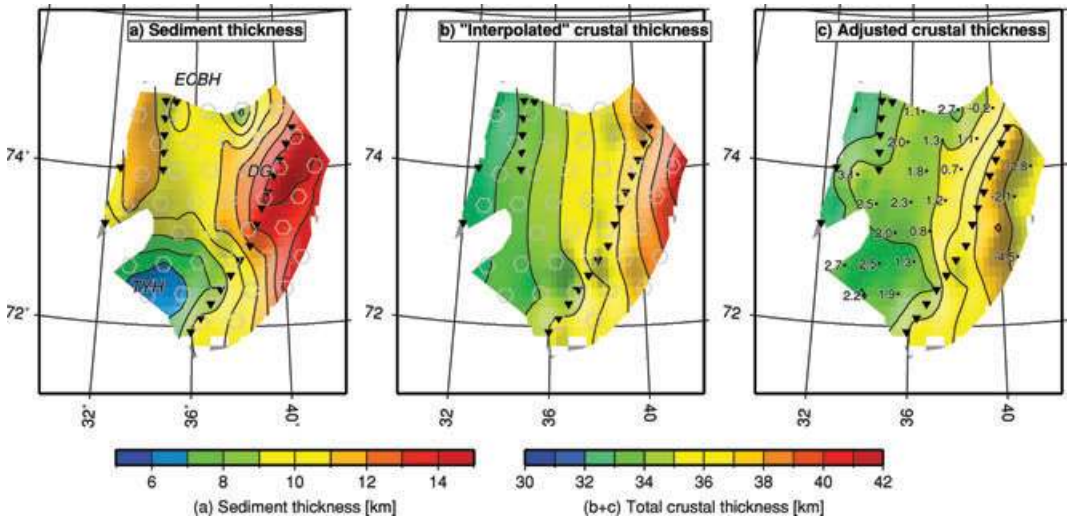

Figure 10. Effect of the thickness adjustments, Central Barents Sea High province. (a) Sediment thickness in the province 17 (Fig. 7), Central Barents Sea High. ECBH, East Barents Sea High; DG, Denisov High; TYH, Tiddlybanken High. (b) Interpolated crustal thickness. (c) Adjusted crustal thickness using the thickness relations. Values are adjustments in (km). Black inverted triangles are database input profiles. Model nodes are indicated by grey hexagons. The complex crustal properties between the two profiles are unknown. A simple interpolation of the crustal thickness results in an unlikely crustal thickness (b) with respect to the sediment thickness (a). The thickness adjustments based on the sediment thickness approximate local compensation (c).

5.2 Crustal model comparisons

To demonstrate the improvements of the newly developed BARENTS50 model we have compared it to commonly applied 3-D models. To this end, Fig. 11 shows the (one-way) traveltimes of seismic *P*-waves from sea level down to the Moho discontinuity in comparison to 3SMAC (Nataf & Ricard 1996), CRUST2.0 (Bassin *et al.* 2000) and WENA1.0 (Pasyanos *et al.* 2004). These illustrations represent the expected traveltime delay for incoming seismic waves caused by the relatively low seismic velocities of the crust compared to the mantle.

The most significant improvement is the increased resolution of 50 km (Fig. 11a) compared to the very smooth fields derived from other models. Generally, the defined geological provinces (Fig. 6a) have a strong effect on the traveltime distribution. Strong gradients in the traveltime are achieved if neighbouring provinces are very different in the calculated regression (Fig. 7). The large traveltime obtained at 73°N/40°E is located at a prominent change of the heading along the profile AR-1 by Sakoulina *et al.* (2003). This is the only location where the traveltime map (Fig. 11a) reflects the input data distribution (Fig. 2). Here, we did not adjust the crystalline crustal thicknesses, since nearby data constraints were given. The total thicknesses of surrounding non-constrained nodes were inferred from the linear relationship shown in Fig. 7 (17, Central Barents High). Therefore, we regard this local 'anomaly' as correct.

The western continent–ocean transition (COT) is clearly visible in the BARENTS50 model, here the traveltimes drop from about 5 to 4 s towards the west. The WENA1.0 model (Fig. 11b) shows the COT similar to our model, although the Moho is about 1.0 s deeper. Local positive undulations in the traveltimes along the COT in the CRUST2.0 model (Fig. 11c) are most likely due to local deposition centres and high accumulation of glacial sediments, which have no traveltime effect in the BARENTS50 model. The average traveltime in the western Barents Sea is about 5.0 s and slightly higher in the east (*ca*. 6.0–6.5 s; Fig. 11a). This trend is approximately matched by the CRUST2.0 model. The 3SMAC shows a strong positive traveltime anomaly on the central Barents shelf (Fig. 11d). The Barents Sea is represented by a 1-D structure in the WENA1.0 model so that local anomalies are absent. Onshore Fennoscandia, 3SMAC and CRUST2.0 match the trend of lower traveltimes in the Caledonian Orogen and towards the Kola Peninsula; again, WENA1.0 incorporates an average model that does not account for regional features of 200–400 km width. Prominent differences between all models occur in the region of the Novaya Zemlya Fold Belt and the Kara Sea. While 3SMAC shows no N–S striking anomalies along Novaya Zemlya, the other models obviously account for the structure of the foldbelt. WENA1.0 shows large mismatches of more than 3.0 s relative to BARENTS50. The traveltimes of more than 8 s are due to a crustal thicknesses of 47 km.

5.3 Basement characterization

Transects through the 3-D velocity model reveal for the first time simplified geological sections through the European Arctic from the Norwegian-Greenland Sea, across the continental margin, to the Barents Sea, the Novaya Zemlya Foldbelt and into the Kara Sea region. The 3-D construction of the sedimentary basins can be interpreted with the crystalline crustal units and Moho topography below, while the seismic velocity distribution sheds light on the possible petrology. Fig. 12 shows transects through BARENTS50 and Fig. 13 shows the depth-to-Moho.

5.3.1 The Barents Sea surroundings

The gabbroic lower crustal layer 3 and the sedimentary cover of the oceanic crust in the Norwegian-Greenland Sea thin with increasing latitude (Fig. 12; province 26). Our model is generally consistent with the results of the crustal studies of Breivik *et al.* (2003) and Ritzmann *et al.* (2004) at the latitudes of Bjørnøya and northern Svalbard, respectively. The upper-oceanic layer 2 remains approximately constant in thickness. This suggests that magmatic activity at the oceanic spreading centre is decreased with decreasing spreading rates in the narrow corridor between Eurasia and Greenland.

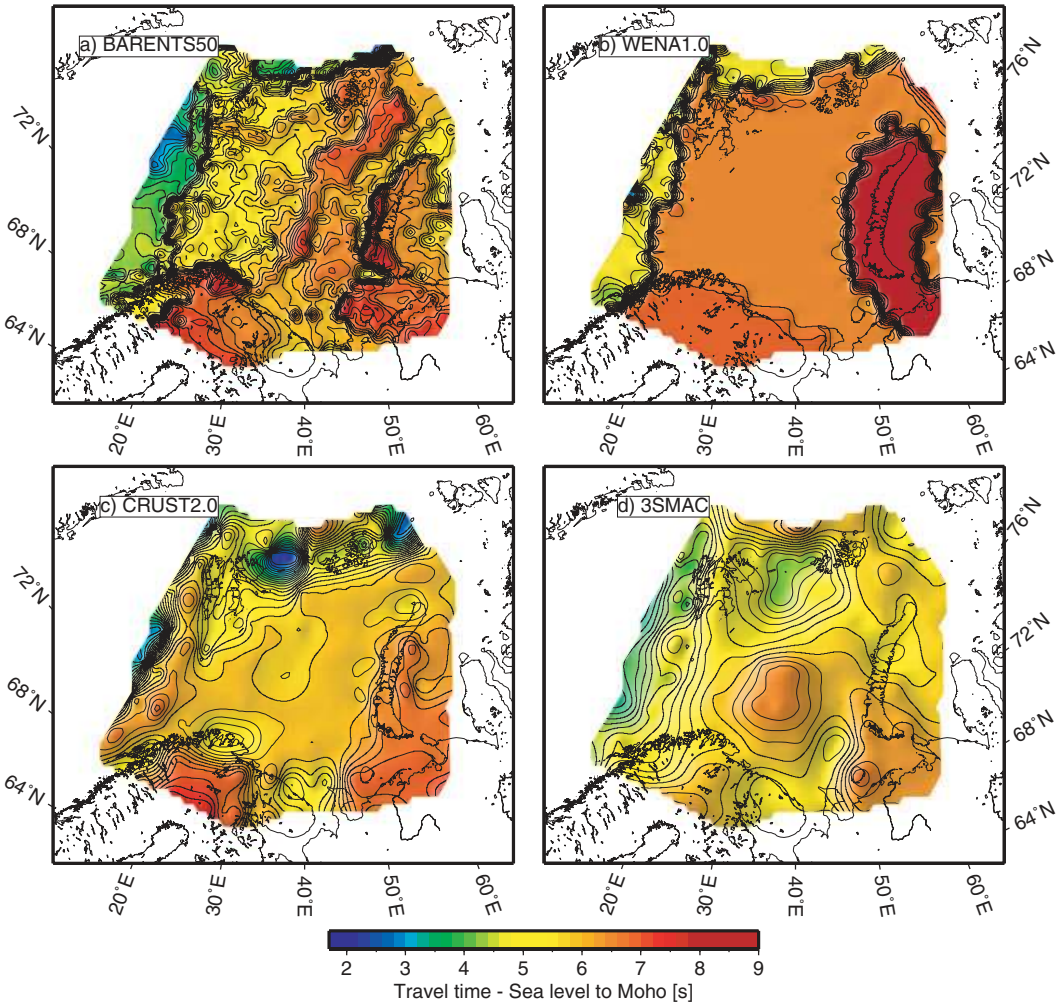

Figure 11. Model comparisons, traveltime to Moho. Traveltimes down to the Moho discontinuity. (a) BARENTS50, this study. (b) WENA1.0 (Pasyanos *et al.* 2004). (c) CRUST2.0 (Bassin *et al.* 2000). (d) 3SMAC (Nataf & Ricard 1996).

Therefore, the traveltime through the crust- and water-column is *ca*. 1 s higher in the south off the western Barents Sea (Fig. 11a).

The Barents Sea is surrounded by thick crustal complexes to the south (Fig. 12; 1, Caledonian Foldbelt; 2, Fennoscandia) and east (20, Novaya Zemlya Foldbelt; 6, Novaya Zemlya Microplate). The crust of the Novaya Zemlya Microplate thins rapidly towards the east, indicating a transition to the Kara Sea province in the east (province 12), where the Moho topography is very rough and characterized by local domes (Fig. 13). These strong lateral thickness variations are well constrained by the seismic velocity models compiled during this study (Fig. 2) and documented by the low slope in the thickness relationship of the Kara Sea province (Fig. 7).

The continental crust of northern Norway and the Kola Peninsula shows similar large thicknesses. In Fennoscandia the maximum Moho depth of 52.4 km is observed. The crustal thicknesses are also in agreement with results from unpublished receiver function analyses of the MASI99 experiment in northern Norway (Hoehne 2001). The majority of the stations derived similar thicknesses, within a range of 1–3 km, to our model. Larger deviations are given in the northern coastal areas where receiver function analyses indicate shallower depths of about 40 km, where our model is contrained by the FENNOLORA-experiment by Guggisberg *et al.* (1991) and the work of Helminsen (2002).

5.3.2 Western Barents Sea (Caledonian) basement

Transect 20 shown in Fig. 12 is subparallel to the geological transect shown in Fig. 1. Breivik *et al.* (2002) suggested a Caledonian suture through the crystalline middle and lower crust separating two distinct basement provinces in the northern Barents Sea. The proposed suture has an apparent dip to the east in Fig. 1 and is thought to include oceanic terrain with higher density. This lineament is well preserved as an east-dipping mid-crustal layer boundary; although the seismic velocities in the lower crust are slightly lower than 6.8 km s^{-1} (provinces 8, 4 and 9). The transects further to the south show a similar, east-dipping boundary separating a nearly similar velocity structure; most likely, the southward continuation of the proposed suture (provinces 5 and 17). This crustal boundary is preserved across province boundaries, which provides additional confidence in the model compilation method.

The average crustal petrology to the east of the suture (the obducted complex) is probably more felsic, since the velocity–depth functions match those with a higher SiO_2-content measured by Christensen & Mooney (1995). Possible igneous to medium-grade metamorphic rocks that match the modelled seismic velocities are granite-granodiorites or granite-gneisses. Since the suturing was probably accompanied by higher-grade metamorphism, a likely

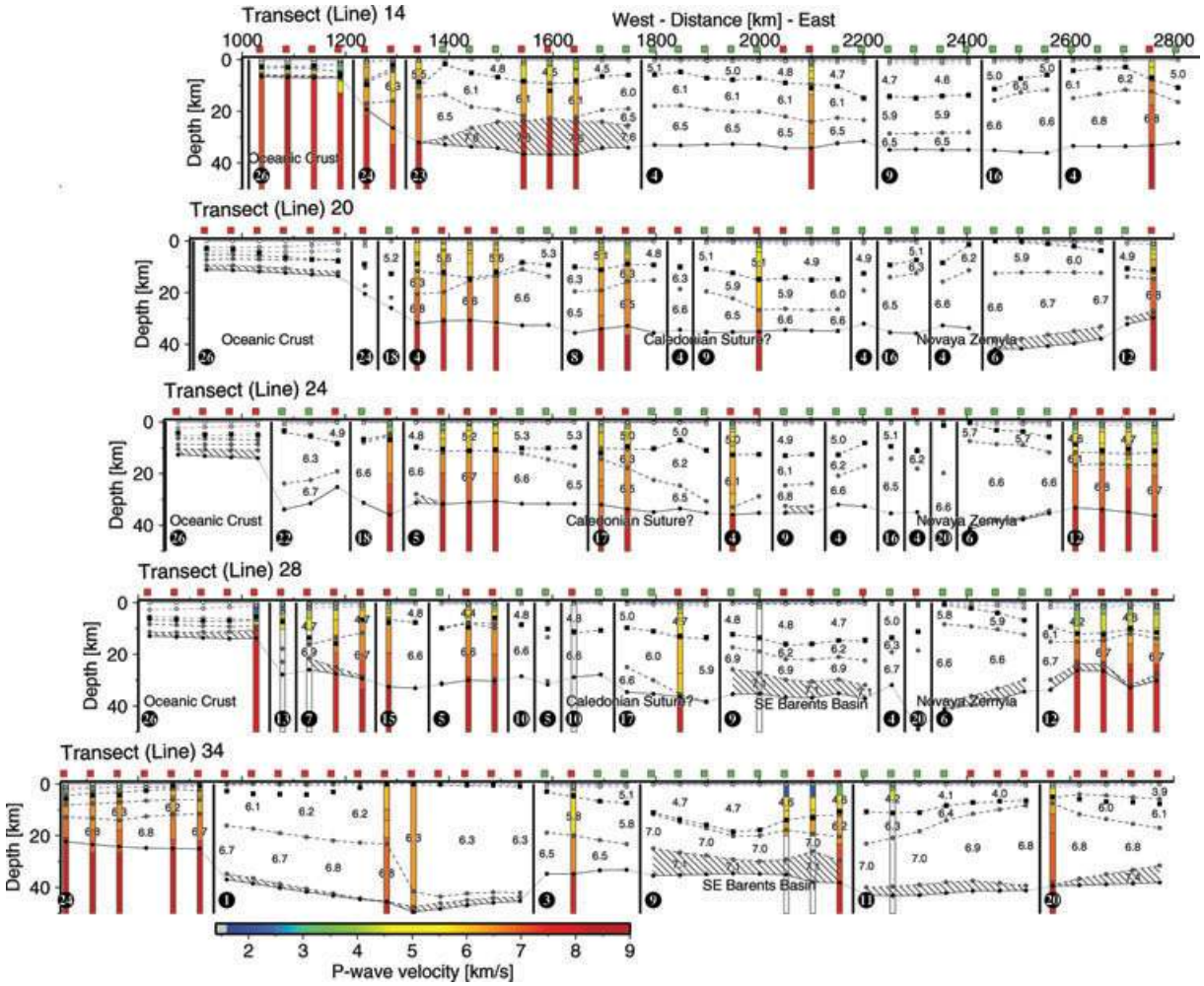

Figure 12. Five crustal transects through the final velocity model. The transects strike west-east and follow the model nodes along the lines 14, 20, 24, 28 and 34 (see Fig. 7b for location). The tops of the two sediment layers are indicated by a blue dashed line, while the three tops of crystalline crustal layers are black-dashed. The lowermost shown layer (solid black line) is the Moho discontinuity. All upper- and lower-layer boundaries at a model node are indicated by a black dot. Red coloured boxes indicate that no thickness adjustments were made, while a green-box-column is adjusted. *P*-wave velocities are plotted along the profile where possible. If the velocity of the lower crystalline crust is >7 km s^{-1} the layer is hatched. Thick vertical black lines show province boundaries along the profiles (Fig. 6a), encircled numbers give the respective province code. In the background of the velocity model, shown as coloured vertical bars, are 1-D velocity profiles from the database (see colour scale).

component of the average crustal petrology is paragranulite, which also falls within the observed seismic velocity range. The crustal structure to the west (the subducted complex) is probably slightly more mafic in character. The observed velocities in the lowermost crust match those of mafic granulites or anorthositic granulites if very high temperatures (645–780°C at 25–30 km depth) are assumed. At lower temperatures, igneous rocks have lower or higher seismic velocities (Christensen & Mooney 1995). A mafic rock composition for the suture zone was also favoured by Breivik *et al.* (2002) on the basis of *P*-wave velocity–density and V_p/V_s ratios. However, our model reveals no clear compositional difference. Even though they petrologically may be quite different, the Caledonian basement provinces on either side of the proposed suture cause no pronounced one-way traveltime differences (Fig. 11a).

5.3.3 Eastern Barents Sea basement

The East Barents Sea Basin extends more than 1000 km west of Novaya Zemlya (Fig. 1). During the velocity model compilation, this very large basin was treated as a single structure. The majority of 1-D velocity models within this province fit to a similar trend in the sediment-crystalline crust relationships (Fig. 7; 9, East Barents Sea Basin). On the other hand, the subsedimentary velocity structure is different in the south and north. While the southern basin is underlain by a three-layer crust with seismic velocities of 6.2, 6.9–7.0 and 7.1 km s^{-1}, the northern part has a two-layer construction with velocities of 5.9–6.0 and 6.5–6.6 km s^{-1} (Fig. 12). The velocities below the southern basin indicate a high mafic rock composition of the middle and lower crust, according to the velocity–depth relationships of Christensen & Mooney (1995). Regardless of the major rock types (igneous, monomineralic or high-grade metamorphic) the high crustal velocities of the lowermost layer (>6.9 km s^{-1}) indicate SiO_2-poor rocks such as gabbro, hornblendite or mafic garnet-granulite. The middle crustal layer shows significantly lower velocities than the measured average of these rocks. Assuming temperatures of 260–645°C in 10–25 km depth, basalts match the velocity structure the best. Mantle-type rocks, such as dunites or pyroxenites, show even higher velocities in continental regions

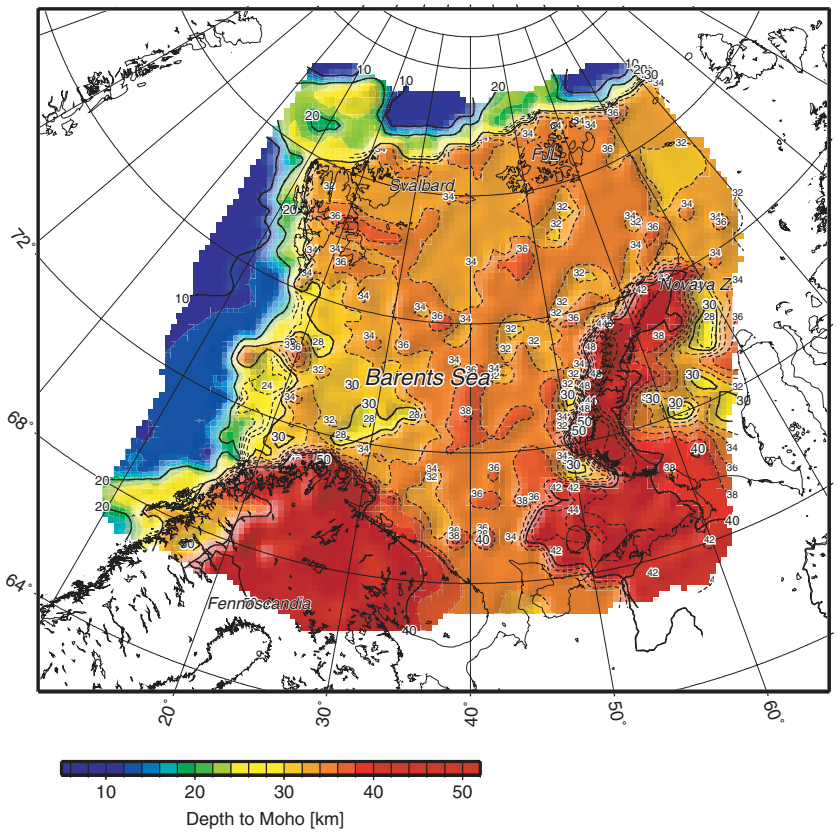

Figure 13. Depth-to-Moho from the BARENTS50 model. Provinces in the central Barents Sea, Novaya Zemlya and Kara Sea show detailed contouring (every 2 km, dashed; other contours: 10 km, solid).

disregarding a possible higher heat flow. Nevertheless, the three-layer construction in the south, the seismic velocity distribution, and the generally thin crystalline crust with almost no Moho topography lead to ideas of a possible suboceanic character which challenge in general the applicability of thickness relationships. Neprochnov *et al.* (2000) concluded on the basis of several studies that the deeply buried high-velocity layers below the southern basin (>7.0 km s^{-1}) may represent a crust–mantle rock mixture in zones of old rifting. Whether this indicates break-up magmatism or incipient seafloor spreading remains uncertain. However, they emphasize the importance of the absence of a (slow and granitic) 6.0–6.2 km s^{-1} layer related to the Baltic Shield in the southern East-Barents Sea Basin, which gets no support from the transects shown in Fig. 12. On the basis of isostatic calculations Artyushkov (2005) excluded oceanic rocks below the very thick sedimentary cover. Instead, he suggests that the deep subsidence is due to a high density and high-grade metamorphic lower crustal layer with a thickness of 15–20 km below the Moho (garnet granulites or eclogites).

The lower velocities in the northern part of the East Barents Sea Basin indicate an average crustal petrology with higher SiO_2-content (e.g. granulites) or effusive mafic rocks (e.g. mafic granulites, basalts or diabases) compared to the southern basin (Christensen & Mooney 1995).

6 CONCLUDING REMARKS

The present study provides a new and detailed crustal velocity model, BARENTS50, for the Barents Sea region with a resolution of 50 km, and with a new compilation strategy based on geological provinces. Other approaches for model compilations using velocity functions from seismic refraction experiments are purely based on mathematical solutions. The fundamental problem of all approaches, including the present one, is the non-uniqueness or ambiguity of the resulting models, which is most striking when using gravity modelling (size and shape of the anomalous body versus its density contrast). In our case, the chosen input are mostly ray tracing based models which are also ambiguous, since traveltime, layer thickness and seismic velocities are convertible parameters. Any geophysical feature of the final constructed model (such as traveltime delays) or geological interpretation (such as the shape and extent of a lower crustal body) are naturally uncertain and, if not treated with care, can lead to false interpretations. However, the principle of layer thickness adjustments based on thickness relationships originated from the detailed analysis of the very simple but consistent data set. The new method for adjusting the crustal thickness was particularly applicable in the Barents Sea region which is largely covered by riftogenic sedimentary basins. At this stage, it remains unclear, however, to what extent this technique is applicable to other regions worldwide.

Our model was already used as primary input for a new surface wave inversion, and along with an extended set of recordings (Levshin *et al.* 2005), improved the mantle model comprehensively. In addition, the model provides assistance for studies of various geodynamic problems concerning the plate tectonic setting of the Barents Sea region, basin formation processes or the distribution of magmatism. Studies of the regional isostatic and thermal states and local gravity and basin modelling are supported thanks to the availability of a complete lithosphere model.

In conclusion, the combination of a consistent seismic database and a reliable methodology to use secondary geological constraints (regional sediment thickness maps and thickness relations) helped significantly to establish a new higher-resolution geophysical model of the greater Barents Sea region.

The velocity model BARENTS50 is available at http://www.norsar.no/seismology/barents3d/

ACKNOWLEDGMENTS

Our study was funded by the U.S. Department of Energy through the National Nuclear Security Administration (DE-.FC52-03NA99508, DE-FC52-03NA99509, DE-FC52-03NA99531), and further initiated by William B. Leith. The depth-to-basement data processed by R. Myklebust was based on the MMBS project of Amarok A.S. [now TGS-NOPEC, in cooperation with the University of Oslo, Sevmorgeo, GECO, the Norwegian Geological Survey (NGU), the University of Copenhagen, and the Norwegian Petroleum Directorate (NPD)]. Special thanks go to N.M. Shapiro and A.L. Levshin who carried out a new 3-D surface wave inversion in the Barents Sea region using our compiled crustal velocity model. The refined upper-mantle velocity model was finally included in our model. Thanks for the detailed comments and suggestions of the two anonymous reviewers and Richard England. Additional thanks go to J. Schweitzer and C. Weidle.

REFERENCES

Artyushkov, E.V., 2005. The formation mechanism of the Barents Basin, *Russ. Geol. Geophys.,* **46**(7), 700–713.

Azbel, I.Ya., Buyanov, A.F., Ionkis, V.T., Sharov, N.V. & Sharova, V.P., 1989. Crustal structure of the Kola Peninsula from inversion of deep seismic sounding data, *Tectonophysics,* **162,** 87–99.

Barton, P.J., 1986. The relationship between velocity and density in the continental crust—a useful constraint?, *Geophys. J. R. astr. Soc.,* **87,** 195–208.

Bassin, C., Laske, G. & Masters, G., 2000. The current limits of resolution for surface wave tomography in North America, *EOS, Trans. Am. geophys. Un.,* **81,** F879.

Bogatsky, V.I., Bogdanov, N.A., Kostyuchenko, S.I., Senin, B.V., Sobolev, S.F., Shipilov, E.V. & Khain, V.E., 1996. Explanatory notes to supplement the tectonic map of the Barents Sea and the northern part of European Russia. Institute of the Lithosphere, Russian Academy of Science, Moscow, Russia.

Bogolepov, A.K., Golionko, G.B. & Nechkhayev, S.A., 1990. Deep geological structure of the Kara Sea, *Sov. Geol. Geophys.,* **31**(6), 25–31.

Breivik, A.J., Gudlaugsson, S.T. & Faleide, J.I., 1995. Ottar Basin, SW Barents Sea: a major Upper Palaeozoic rift basin containing large volumes of deeply buried salt, *Basin Research,* **7,** 299–312.

Breivik, A.J., Faleide, J.I. & Gudlaugsson, S.T., 1998. Southwestern Barents Sea margin: late Mesozoic sedimentary basins and crustal extension, *Tectonophysics,* **293,** 21–44.

Breivik, A.J., Verhoef, J. & Faleide, J.I., 1999. Effect of thermal contrasts in gravity modeling at passive margins: results from the western Barents Sea, *J. geophys. Res.,* **104**(B7), 15 293–15 311.

Breivik, A.J., Mjelde, R., Grogan, P., Shimamura, H., Murai, Y., Nishimura, Y. & Kuwano, A., 2002. A possible Caledonide arm through the Barents Sea imaged by OBS data, *Tectonophysics,* **355,** 67–97.

Breivik, A.J., Mjelde, R., Grogan, P., Shimamura, H., Murai, Y. & Nishimura, Y., 2003. Crustal structure and transform margin development south of Svalbard on ocean bottom seismometer data, *Tectonophysics,* **369,** 37–70.

Breivik, A.J., Mjelde, R., Grogan, P., Shimamura, H., Murai, Y. & Nishimura, Y., 2005. Caledonide development offshore-onshore Svalbard based on ocean bottom seismometer, conventional seismic and potential field data, *Tectonophysics,* **401,** 79–117.

Christensen, N.I. & Smewing, J.D., 1981. Geology and seismic structure of the northern section of the Oman Ophiolite, *J. geophys. Res.,* **86**(B4), 2545–2555.

Christensen, N.I. & Mooney, W.D., 1995. Seismic velocity structure and composition of the continental crust: a global view, *J. geophys. Res.,* **100**(B7), 9761–9788.

Dibner, V.D., 1998. The geology of Franz Josef Land, in *Geological aspects of Franz Josef Land and the northernmost Barents Sea—The northern Barents Sea Geotraverse*, Vol. 151, pp. 10–17, eds Solheim, A., Musatov, W. & Heintz, N., Norsk Polarinstitutt Meddelelser, Tromsø, Norway.

Dimakis, P., Braathen, B.I., Faleide, J.I., Elverhoi, A. & Gudlaugsson, S.T., 1998. Cenozoic erosion and the preglacial uplift of the Svalbard-Barents Sea region, *Tectonophysics,* **300,** 311–327.

Dobrhzhinetskaya, L.F., Nordgulen, Ø., Vetrin, V.R., Cobbing, J. & Sturt, B.A., 1995. Correlation of the Achean rocks between the Sørvaranger area, Norway and the Kola Peninsula, Russia (Baltic Shield), *Nor. Geol. Unders. Special Publ.,* **7,** 7–27.

Egorkin, A.V., 1991. Crustal structure from seismic long-range profiles, in *Deep structure of the Territory of the USSR*, pp. 118–134, ed. Beloussov, V.V., Nauka, Moscow.

Engen, Ø., 2005. Evolution of High Arctic Ocean Basins and Continental Margins. *PhD thesis*, Department of Geosciences, University of Oslo, Oslo, Norway.

Faleide, J.I., Gudlaugsson, S.T., Eldholm, O., Myhre, A.M. & Jackson, H.R., 1991. Deep seismic transects across the sheared western Barents Sea-Svalbard continental margin, *Tectonophysics,* **189,** 73–89.

Faleide, J.I., Vagnes, E. & Gudlaugsson, S.T., 1993. Late Mesozoic-Cenozoic evolution of the south-western Barents Sea in a regional rift-shear tectonic setting, *Mar. Petr. Geol.,* **10,** 186–214.

Geissler, W.H., 2001. Marine seismische Untersuchungen am nördlichen Kontinentalrand von Svalbard (Spitzbergen). *Unpublished diploma thesis*, Institut für Geophysik der Technischen Universität Bergakademie Freiberg, Freiberg.

Grogan, P., Nyberg, K., Fotland, B., Myklebust, R., Dahlgren, S. & Riis, F., 1998. Cretaceous magmatism south and east of Svalbard; evidence from seismic reflection data, in *Proceedings of the ICAM III, Third International Conference on Arctic Margins*, Vol. 68, pp. 25–34, eds Roland, R.N. & Tessensohn, F., Polarforschung, DGP, Frankfurt, Germany.

Gudlaugsson, S.T., Faleide, J.I., Fanavoll, S. & Johansen, B., 1987. Deep seismic reflection profiles across the western Barents Sea, *Geophys. J. R. astr. Soc.,* **89,** 273–278.

Gudlaugsson, S.T., Faleide, J.I., Johansen, S.E. & Breivik, A.J., 1998. Late paleozoic structural development of the South-western Barents Sea, *Mar. Petr. Geol.,* **15,** 73–102.

Guggisberg, B., Kaminski, W. & Prodehl, C., 1991. Crustal structure of the Fennoscandian Shield; a traveltime interpretation of the long-range FENNOLORA seismic refraction profile, *Tectonophysics,* **195,** 105–137.

Harland, W.B. (with a contribution of Nicholas J. Butterfield), 1997. Pre-Vendian history, in *The Geology of Svalbard*, Vol. 17, pp. 227–243, ed. Harland, W.B., Geol. Soc. Mem., The Geological Society, London

Helminsen, L., 2002. Skorpestuktur i Finnmark og det sydvestlige Barentshav, *Unpublished Master thesis,* Geological Department, University of Oslo, Oslo.

Hoehne, J., 2001. Untersuchungen der Geschwindigkeitsstruktur der Kruste und des oberen Mantels der Finnmark aus den Daten des MASI 99 Projektes, *Unpublished diploma thesis*, Institut für Geowissenschaften, Fachbereich Geophysik, Universitaet Potsdam, Potsdam.

Høgden, S., 1999. Seismotectonics and crustal structure of the Svalbard Region, *Unpublished Master thesis,* Geological Department, University of Oslo, Oslo.

Jackson, H.R. (compiler), 2002. Arctic Refraction Catalogue of the Geological Survey of Canada, http://gsca.nrcan.gc.ca/databases/arctic/index˙e.php.

Jackson, H.R., Faleide, J.I. & Eldholm, O., 1990. Crustal structure of the sheared southwestern Barents Sea continental margin, *Mar. Geol.,* **93,** 119–146.

Johansen, S.E. *et al.*, 1993. Hydrocarbon potential in the Barents Sea region: play distribution and potential, in *Arctic geology and petroleum potential*, Vol. 2, pp. 273–320, eds Vorren, T.O., E., Bergsaker, Ø. A. Dahl-Stamnes, E., Holter, B. Johansen, E., Lie, & T.N. Lund, NPF Special Publication, Elsevier, New York.

Kanestrøm, R., 1971. Seismic investigations of the crust and upper mantle in Norway, in *Proc. Colloq. Deep Seismic Sounding in Northern Europe*, Vol. 1969, pp. 17–27, ed. Vogel, A., Upsala, Dec. 1–2, Swedish Natural Science Research Council, Stockholm.

Kimbell, G.F., Gadliff, R.W., Ritchie, J.D., Walker, A.S.D. & Williamson, J.P., 2004. Regional three-dimensional gravity modelling of the NA Atlantic margin, *Basin Res.,* **16,** 259–278.

Kodaira, S. *et al.*, 1995. Crustal structure of the Lofoten continental margin, off Northern Norway, from ocean-bottom seismograph studies, *Geophys. J. Int.,* **121,** 907–924.

Kostyuchenko, S.L., Egorkin, A.V. & Solodilov, L.N., 1999. Structure and genetic mechanisms of the Precambrian rifts of the East-European Plarform in Russia by integrated study of seismic, gravity, and magnetic data, *Tectonophysics,* **313,** 9–28.

Kremenetskaya, E., Asming, V. & Ringdal, F., 2001. Seismic location calibration of the European Arctic, *Pure appl. Geophys.,* **158,** 117–128.

Levshin, A., Schweitzer, J., Weidle, C., Maercklin, N., Shapiro, N. & Ritzwoller, M., 2005. Surface wave tomography of the European Arctic, *EOS, Trans. Am. geophys. Un.,* **86** (52), Fall Meet. Suppl., Abstract S51E-1053.

Ljones, F., Kuwano, A., Mjelde, R., Breivik, A., Shimamura, H., Murai, Y. & Nishimura, Y., 2004. Crustal transect from the Knipovich Ridge to the Svalbard Margin west of Hornsund, *Tectonophysics,* **378,** 17–41.

Ludwig, J.W., Nafe, J.E. & Drake, C.L., 1970. Seismic refraction, in *The Sea*, Vol. 4, pp. 53–84, ed. Maxwell, A.E., Wiley-Interscience, New York.

Luosto, U., Flueh, E.R. & Lund, C.-E., 1989. The crustal structure along the POLAR profile from seismic refraction investigations, *Tectonophysics,* **162,** 51–85.

McCowan, D.W., Glover., P. & Shelton, S.A., 1978. A crust and upper mantle model for Novaya Zemlya from Rayleigh wave dispersion data, *Bull. seism. Soc. Am.,* **68**(6), 1651–1662.

McKenzie, D., 1978. Some remarks on the development of sedimentary basins, *Earth planet. Sci. Lett.,* **40,** 25–32.

Mjelde, R., Sellevoll, M.A., Shimamura, H., Iwasaki, T. & Kanazawa, T., 1992. A crustal study off Lofoten, N., Norway, by use of 3-component Ocean Bottom Seismographs, *Tectonophysics,* **212,** 269–288.

Mjelde, R., Kodaira, S. & Sellevoll, M.A., 1996. S-wave structure of the Lofoten Margin, N., Norway, from wide-angle data: a review, *Norsk Geologisk Tidsskrift,* **76,** 231–244.

Mjelde, R. *et al.*, 2002. Geological development of the Sørvestnaget Basin, SW Barents Sea, from ocean-bottom seismic, surface seismic and potential field data, *Norsk Geologisk Tidsskrift,* **82**(3), 183–202.

Mosar, J., Eide, E.A., Osmundsen, P.T., Sommorugo, A. & Torsvik, T.H., 2002. Greenland-Norway separation: a geodynamic model for the North Atlantic, *Norsk Geologisk Tidsskrift,* **82**(4), 281–298.

Mooney, W.D., Laske, G. & Masters, T.G., 1998. CRUST5.1: a global crustal model at $5^\circ \times 5^\circ$, *J. geophys. Res.,* **103**(B1), 727–747.

Myklebust, R., 1994. Magentic mapping of the Barents Sea (MMBS)—Interpretation report. Unpublished Report, Amarok A.S., Oslo, Norway.

Nataf, H.-C. & Ricard, Y., 1996. 3SMAC: an a priori tomographic model of the upper mantle based on geophysical modeling, *Phys. Earth planet. Inter.,* **95,** 101–122.

Neprochnov, Yu.P., Semenov, G.A., Sharov, N.V., Yliniemi, J., Komminaho, K., Luosto, U. & Heikkinen, P., 2000. Comparision of the crustal structures of the Barents Sea and the Baltic Shield from seismic data, *Tectonophysics,* **321,** 429–447.

O'Leary, N., White, N., Tull, S., Bashiov, V., Kuprin, V., Natapov, L. & Macdonald, D., 2004. Evolution of the Timan-Pechora and South Barents Sea basins, *Geol. Mag.,* **141**(2), 141–160.

Pasyanos, M.E., Walter, W.R., Flanagan, M.P., Goldstein, P. & Bhattacharyya, J., 2004. Building and testing an a priori Geophysical Model for western Eurasia and North Africa, *Pure appl. Geophys.,* **161,** 235–281.

Pentilla, E., 1971. Seismic investigations on the Earth's crust in Finland, in ed.Vogel, A., *Proc. Colloq. Deep seismic sounding in Northern Europe*, Upsala, Dec. 1–2, 1969, 9–13, Swedish Natural Science Research Council, Stockholm.

Plouff, D., 1976. Gravity and magnetic fields of polygonal prisms and application to magnetic terrain corrections, *Geophysics,* **41,** 727–741.

Puchkov, V.N., 1996. Formation of the Urals-Novaya Zemlya Foldbelt; a result of irregular oblique collision of the continents, *Geotectonics,* **30,** 400–409.

Ramsay, D.M., Sturt, B.A., Zwann, K.B. & Roberts, D., 1985. Caledonides of northern Norway, in *The Caledonian Orogen—Scandinavia and Related Ares*, Part 1, pp. 163–184, eds Gee, D.G. & Sturt, B.A., John Wiley & Sons, Chichester.

Ritzmann, O., 2003. Architechture and geodynamic evolution of the Svalbard Archipelago, the Yermak Plateau and the Fram Strait oceanic Province from deep seismic experiments, *Reports on Polar and Marine Research*, **439,** 143 pp.

Ritzmann, O. & Jokat, W., 2003. Crustal structure of northwestern Svalbard and the adjacent Yermak Plateau: evidence for Oligocene detachment tectonics and non-volcanic break-up, *Geophys. J. Int.,* **152,** 139–159.

Ritzmann, O., Jokat, W., Mjelde, R. & Shimamura, H., 2002. The crustal structure between the Knipovich Ridge and the Van Mijenfjorden, *Mar. Geophys. Res.,* **23** (5–6), 379–401.

Ritzmann, O., Jokat, W., Czuba, W., Guterch, A., Mjelde, R. & Nishimura, Y., 2004. A deep seismic transect in northwestern Svalbard at Kongsfjorden (Ny Ålesund) and the implications for Cenozoic break-up from Greenland: A sheared margin study, *Geophys. J. Int.* **157,** 683–702.

Roberts, D. & Gee, D.G., 1985. An introduction to the structure of Scandinavia Caledonides, in *The Caledonian Orogen—Scandinavia and related areas*, Part 1, pp. 55–68, eds Gee, D.G. & Sturt, B.A., John Wiley & Sons, Chichester.

Sakoulina, T.S., Roslov, Yu.V. & Ivanova, N.M., 2003. Deep seismic investigations in the Barents and Kara seas, *Rus. Acad. Sci. Phys. Solid Earth,* **39**(6), 438–452.

Sanner, S., 1995. Et seismisk hastighetsstudium i Barentshavet, *Unpublished Master thesis,* Geological Department, University of Oslo, Oslo, p. 149.

Schweitzer, J. & Kennett, B.L.N., 2002. Comparison of local procedures - The Kara Sea event 16 August 1997, *Norsar Sci. Rep. 1-2002,* 97–114.

Sellevoll, M.A., 1983. A study of the Earth's crust in the island area of Lofoten-Vesterålen, Northern Norway, *Norges Geologiske Undersøkelse Bulletin,* **380,** 235–243.

Shapiro, N.M. & Ritzwoller, M.H., 2002. Monte-Carlo inversion for a global shear velocity model of the crust and upper mantle, *Geophys. J. Int.,* **151,** 88–105.

Sigmond, E.M.O., 2002. Geologisk Kart over land- og havområder i Nordeuropa, målestokk 1:4000000. Norges geologiske undersøkelse, Trondheim.

Smith, W.H.F. & Wessel, P., 1990. Gridding with continuous curvature splines in tension, *Geophysics,* **55**(3), 293–305.

Verba, M.L., Daragan-Sushchova, L.A. & Pavlenkin, A.D., 1992. Riftogenic structures of the western arctic shelf investigated by refraction studies, *Int. Geol. Rev.,* **34**(8), 753–764.

Vol'vovskiy, I.S. & Vol'vovskiy, B.S., 1975. Cross-sections of the Earth's crust on the territory of the USSR, as inferred from deep-seismic sounding data. (In the collection: Rezul'taty issledovaniy po mezhdunarodnym geofizicheskim proyektam), Sov. radio. Mocscow, p. 256.

Walther, C. & Flueh, E.R., 1993. The POLAR profile revisited; combined *P*- and *S*-wave interpretation, *Precambrian Res.,* **64,** 153–168.

Watts, A.B., 2001. *Isostasy and Flexure of the lithosphere*, Cambridge University Press, Cambridge, 458 pp.

Zonenshain, L.P., Kuzmin, M.I. & Natapov, L.M., 1990. Geology of the USSR: a plate tectonic sythesis. Geodynamic Series 21, Americam Geophysical Union, Washington, DC.